

113  
19  
C.

GEOCHEMISTRY OF SOUTHWESTERN NEW MEXICO FLUORITE DEPOSITS;  
POSSIBLE BASE AND PRECIOUS METALS EXPLORATION SIGNIFICANCE

by

**NMIMT**  
**Library**  
**SOCORRO, NM**

Gregory T. Hill

Submitted in Partial Fulfillment of the  
Requirements for the Degree of  
Master of Science

New Mexico Institute of Mining and Technology  
Socorro, NM

4 October 1994

32101650

## ABSTRACT

Fluorite is present as a gangue or associated mineral in many epithermal base and precious metal vein and replacement deposits occurring in a wide variety of host lithologies. It also forms in many barren deposits under a diverse set of geological and geochemical conditions. Because fluorite contains trace and rare earth elements, and contains neither oxygen nor hydrogen, several geochemical parameters including fluorite composition, fluid inclusion microthermometry, and  $\delta D$  and  $\delta^{18}O$  values of inclusion fluids in fluorite can be used to compare and contrast barren and metalliferous deposits. The aim of this study is to assess the potential of using fluorite geochemistry as an exploration tool in the search for base and/or precious metals mineralization. Southwestern New Mexico contains many varieties of both barren and metalliferous deposits and was therefore chosen as a field area.

Fluid inclusion microthermometry indicates that most of the fluorite deposits formed from low salinity (0 - 7 eq. wt.% NaCl) fluids at temperatures between 100 and 220 °C. A small number of deposits, including the Hansonburg MVT deposit, formed from higher salinity fluids (10-20 eq. wt.% NaCl) at temperatures between 100 and 200 °C.  $\delta D$  and  $\delta^{18}O$  values of inclusion fluids range respectively from -108 to -27 permil and -9.9 to 5 permil relative to SMOW. Horizontal to sub horizontal trends on a  $\delta D$  versus  $\delta^{18}O$  diagram suggest

that variably-exchanged meteoric waters were responsible for fluorite deposition in most deposits. However, a small component of magmatic fluids can not be ruled out in most districts.

The rare earth elements (REE) show a broad range in concentration with individual REE ranging from tenths to tens of part per million. REE compositions of fluorites generally reflect the various lithologies which host fluorite mineralization. Igneous-hosted fluorite tends to have high  $\Sigma$ REE content relative to sediment-hosted fluorite. Furthermore, granite-hosted fluorites are enriched in HREE over LREE. Thus, fluorites hosted by sedimentary, granitic, and other igneous lithologies can be distinguished from one another.

Small and/or isolated ranges in Sr concentration, Sc/Eu ratio, Tb/Yb ratio, and sign and magnitude of europium anomaly constrain fluorites associated with low salinity base and/or precious metals mineralization. One apparently barren fluorospar district in southwestern New Mexico contains fluorite with signatures indicative of metalliferous mineralization. For this reason, it is suggested that significant base and/or precious metals exploration potential may exist within this district.

## ACKNOWLEDGMENTS

I wish to thank the many people who provided financial, academic, and moral support during my graduate career at New Mexico Tech. Without their support, this project could not have been done. Special thanks to my advisor, Dr. Andrew R. Campbell for his patience, knowledge, and thoughtful review of this thesis. Special thanks also goes to my other committee members, Dr. Philip Kyle and Dr. William X. Chavez, for their support and assistance.

Financial support for this research was provided by several sources including the Geological Society of America, the New Mexico State Mines and Mineral Resources Research Institute, the Charles Park Fellowship, and the Geoscience Department at New Mexico Institute on Mining and Technology. I thank them all sincerely.

Thanks also to the many friends I have made here whose companionship and thought have made this an enjoyable experience. Finally, I wish to thank my mother, without whose long-standing support I could not have done it.

# CONTENTS

	PAGE
ACKNOWLEDGMENTS-----	ii
LIST OF TABLES-----	v
LIST OF FIGURES-----	vi
LIST OF APPENDICES-----	vii
INTRODUCTION-----	1
METHODS-----	4
SAMPLING-----	4
MINERAL SEPARATION TECHNIQUES-----	7
INSTRUMENTAL NEUTRON ACTIVATION ANALYSIS-----	7
X-RAY FLUORESCENCE ANALYSIS-----	8
FLUID INCLUSION MICROTHERMOMETRY-----	8
STABLE ISOTOPE MASS SPECTROMETRY-----	9
GEOLOGY AND MINERALIZATION-----	10
LEMITAR MOUNTAINS DEPOSITS-----	13
GONZALES PROSPECT-----	14
HANSONBURG DISTRICT-----	14
SIERRA CABALLO DEPOSITS-----	15
ORGAN MOUNTAINS DEPOSITS-----	16
SIERRA CUCHILLO DEPOSITS-----	16
CAPITAN MOUNTAINS DEPOSITS-----	17
FLUORITE RIDGE DEPOSITS-----	18
LORDSBURG DISTRICT-----	19
BIG BURRO MOUNTAINS DEPOSITS-----	20
GILA FLUOROSPAR DISTRICT-----	21
STEEPLE ROCK DISTRICT-----	22

## CONTENTS

	PAGE
ACKNOWLEDGMENTS-----	ii
LIST OF TABLES-----	v
LIST OF FIGURES-----	vi
LIST OF APPENDICES-----	vii
INTRODUCTION-----	1
METHODS-----	4
SAMPLING-----	4
MINERAL SEPARATION TECHNIQUES-----	7
INSTRUMENTAL NEUTRON ACTIVATION ANALYSIS-----	7
X-RAY FLUORESCENCE ANALYSIS-----	8
FLUID INCLUSION MICROTHERMOMETRY-----	8
STABLE ISOTOPE MASS SPECTROMETRY-----	9
GEOLOGY AND MINERALIZATION-----	10
LEMITAR MOUNTAINS DEPOSITS-----	13
GONZALES PROSPECT-----	14
HANSONBURG DISTRICT-----	14
SIERRA CABALLO DEPOSITS-----	15
ORGAN MOUNTAINS DEPOSITS-----	16
SIERRA CUCHILLO DEPOSITS-----	16
CAPITAN MOUNTAINS DEPOSITS-----	17
FLUORITE RIDGE DEPOSITS-----	18
LORDSBURG DISTRICT-----	19
BIG BURRO MOUNTAINS DEPOSITS-----	20
GILA FLUOROSPAR DISTRICT-----	21
STEEPLE ROCK DISTRICT-----	22

ZUNI MOUNTAINS FLUOROSPAR DISTRICT-----	23
RESULTS AND DISCUSSION-----	24
FLUID INCLUSIONS-----	24
STABLE ISOTOPES-----	29
TRACE AND RARE EARTH ELEMENTS-----	45
SUMMARY AND CONCLUSIONS-----	63
REFERENCES-----	67
APPENDIX I-----	71
APPENDIX II-----	81
APPENDIX III-----	83
APPENDIX IV-----	86

LIST OF TABLES

	PAGE
Table 1. Deposit descriptions-----	11
Table 2. Rare earth element characteristics-----	52



## LIST OF FIGURES

	PAGE
Figure 1. Sample location map-----	6
Figure 2. Th vs. Salinity diagram-----	28
Figure 3. Salinity and Th histograms-----	31
Figure 4. $\delta D$ vs. $\delta^{18}O$ diagram-----	40
Figure 5. Salinity vs. $\delta^{18}O$ -----	44
Figure 6. Sc vs. Sum of REE diagram-----	47
Figure 7. Sc/Eu ratio vs. Sr diagram-----	50
Figure 8. $(La/Yb)_n$ vs. $(Eu/Eu^*)_n$ diagram-----	54
Figure 9. $(Tb/Yb)_n$ vs. Sum of REE diagram-----	56
Figure 10. $(Ce/Ce^*)_n$ vs. $(Eu/Eu^*)_n$ diagram-----	60

## LIST OF APPENDICES

	PAGE
Appendix I. Fluid inclusion Th and Salinity data-	71
Appendix II. Stable isotope data-----	81
Appendix III. Trace and rare earth element data----	83
Appendix IV. H <sub>2</sub> O/CO <sub>2</sub> microequilibration and uranium reduction procedures-----	86

## INTRODUCTION

Fluorite occurs in a diverse group of mineral deposits with varied host lithologies, mineralogies, and styles of mineralization (Peters, 1958; Richardson and Holland, 1979). Fluorite deposits range from low temperature and low salinity meteoric-hydrothermal veins and replacements to high temperature and high salinity magmatic deposits (Kesler, 1977; Strong and Fryer, 1984, Ekambaram et al., 1986, Akande et al., 1989; Galindo et al., 1994). Fluorite is associated with base and precious metals ores in epithermal, skarn, and porphyry environments.

The ubiquitous occurrence of trace and rare earth elements in fluorite allows for geochemical comparison between a wide variety of deposit types. Through this comparison, fluorite deposits associated with metalliferous mineralization may be distinguishable from those which are not. If this is possible, fluorite geochemistry may be a useful exploration tool in areas where fluorite is associated with base and/or precious metals mineralization. Stable isotopic and microthermometric data, measured from fluid inclusions in fluorite, augment the compositional data by providing genetic information about the fluids from which fluorite was deposited. Combining compositional, isotopic, and microthermometric data allows for an integrated approach to the study of fluorite occurrences.

Southwestern New Mexico was chosen as a field area because of its numerous epithermal fluorite occurrences of

several genetic styles. Base and precious metals have been produced from several types of fluorite-bearing deposits in southwestern New Mexico including MVT deposits, volcanic-hosted epithermal veins, and carbonate-hosted epithermal veins and stratabound replacement deposits. Many apparently barren fluorite-quartz±barite±calcite±sulfide deposits are also present in this region and may host undiscovered metals mineralization (McAnulty, 1978; Rothrock et al., 1946). Barren deposits occur near metalliferous deposits in similar geologic environments along extensional structures associated with basin and range tectonism. Geologic similarities among barren and metalliferous fluorite-bearing deposits suggest that significant potential exists for the discovery of metalliferous orebodies associated with seemingly barren occurrences.

Rare earth element (REE) compositions of fluorites tend to be indicative of their host lithologies and thereby record the environment of formation (Fleischer, 1969). It is likely that controls such as temperature, salinity,  $f_{O_2}$ , and pH also influence fluorite composition. However, because of a lack of experimental data, modeling of these parameters based on fluorite geochemistry is not yet possible. Therefore, this study is necessarily empirical.

#### *Previous work*

In a compilation of fluorite analyses, Fleischer (1969) notes that host lithologies exert strong influences on

fluorite composition. He finds that heavy rare earth elements (HREE) are concentrated in fluorites from granitic pegmatites, while those hosted by alkalic rocks contain light rare earth element (LREE) concentrations. Rare earth element geochemistry has been used as an aid to understanding fluorospar genesis by numerous workers (Moller et al., 1976; Moller and Morteani, 1983; Ekambaram et al., 1986; Ganzeyev and Sotskov, 1976). Schneider et al. (1975) and Moller et al. (1976) discriminate synsedimentary, hydrothermal, and pegmatitic fluorite types using Tb/Ca and Tb/La ratios. Strong et al. (1984) and Constantopoulos (1988) combine REE data with fluid inclusion microthermometry and stable isotope studies as a means of deciphering fluorospar genesis.

Radiogenic isotope studies have proven useful in the study of fluorite mineralization. Strontium isotopes have been used to determine the source of Sr, and by inference Ca, in Mexican fluorospar deposits (Ruiz et al., 1980; Ruiz et al., 1985). Fluorite crystals from Mississippi Valley Type deposits have been age dated by Sm-Nd techniques (Halliday et al., 1990; Chesley et al., 1991). Fluorite deposits in Southwestern New Mexico have not been successfully age dated although field relationships suggest that most are post-Cretaceous in age.

Several studies concerned with the genesis of individual fluorite deposits in New Mexico have been undertaken (North and McLemore, 1985; North and Tuff, 1986;

Gilder, 1989). Eppinger and Closs (1990) use trace and rare earth element compositions of fluorite to discriminate among four types of metalliferous and barren deposit types in Sierra County, New Mexico. They suggest that fluorite composition varies systematically according to deposit type, and may therefore constitute an exploration tool. The present study seeks to expand upon their research by including fluorites from a larger and more geologically diverse region.

## METHODS

### *Sampling*

Grab samples were collected from mine dumps and workings, and outcrops in 12 regions in New Mexico (Figure 1). Care was taken to sample material representative of mineralization at each deposit. Fluorite with iron-oxide staining was avoided whenever possible.

The sample base is broadly representative of the geologic and mineralogic diversity of fluorite deposits in southwestern New Mexico. Large sample sets (5-7 samples) represent deposits in the Capitan Mountains, the Hansonburg district, the Sierra Caballo, and Fluorite Ridge. The Sierra Cuchillo, Gonzales prospect, Zuni Mountains, Gila Fluorospar district, Big Burro Mountains, Lordsburg district, and Organ Mountains deposits are each represented by 2-3 samples. The Lemitar Mountains and Steeple Rock district deposits are represented by one sample each.

Figure 1. Sample location map. Refer to Table 1 for location names.

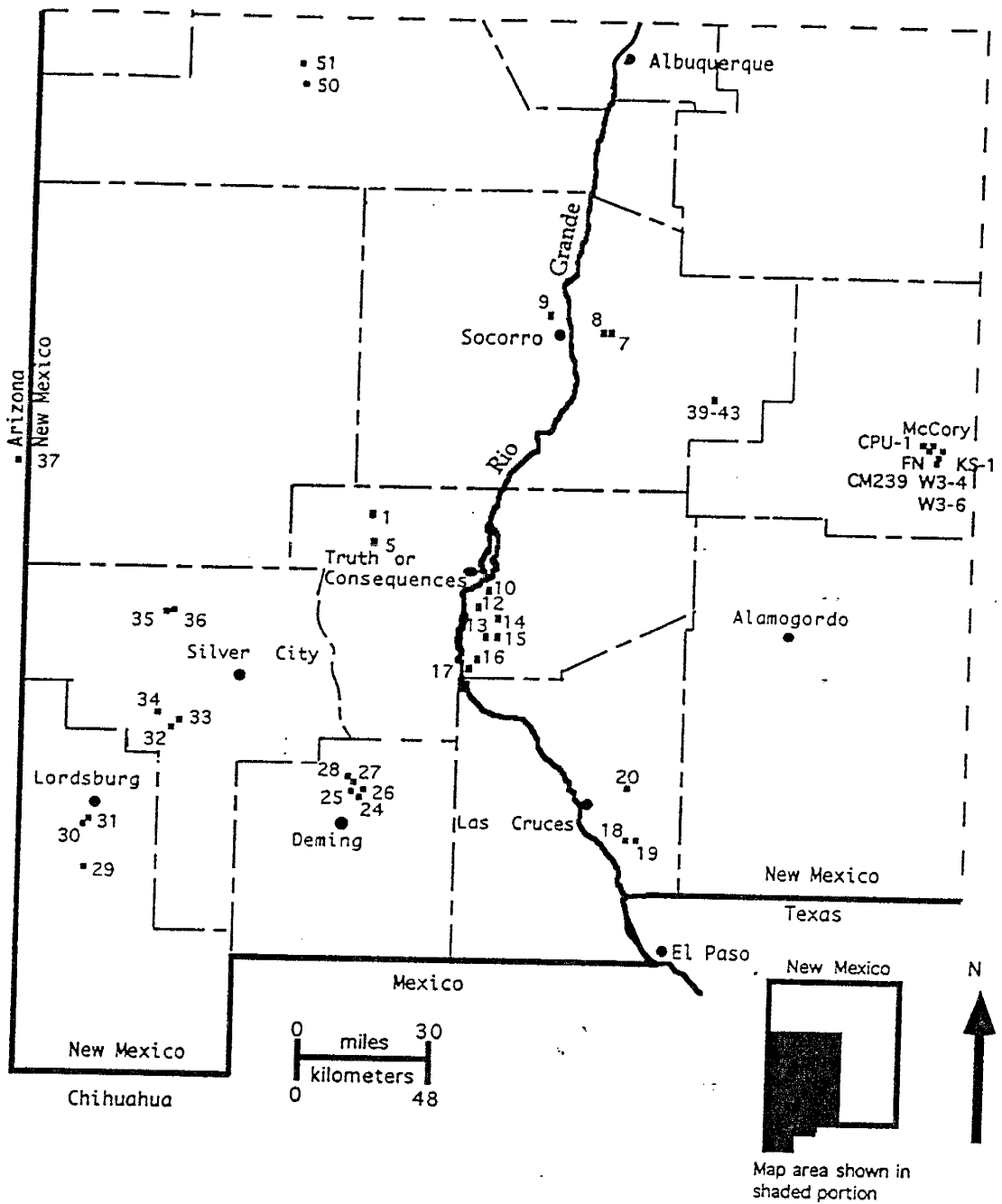


Figure 1. Sample location map.



By comparison to the larger data sets, one can estimate the amount of variability that might exist in districts which are represented by only a small number of samples.

#### *Mineral separation techniques*

Jaw-crushed samples were hand picked for impurities and iron-oxide and manganese-oxide stained fragments. The remaining portions were ground in a TEMA mill and sieved to -10/+40 mesh. This size fraction was hand picked until it contained at least 99% fluorite by visual estimation. The hand picked material was then bathed in warm 10% HCl solution, repeatedly rinsed in distilled H<sub>2</sub>O, and oven dried at low temperature. Samples used for isotope analysis were, in addition, bathed in a 10% NaOH solution, thoroughly rinsed, and oven dried.

#### *Instrumental neutron activation analysis*

Approximately 100 mg fluorite samples were loaded into high-purity silica vials which were then flame sealed and cleaned in acetone. The samples were irradiated at the University of Missouri Research Reactor for a period of 24 hours at a thermal neutron flux of  $2.4 \times 10^{13}$  n cm<sup>-2</sup> sec<sup>-1</sup>. Gamma rays were counted 6-12 days and 30-40 days after irradiation on two high-purity p-type Ge detectors at New Mexico Institute of Mining and Technology. Data was reduced using the TEABAGS (Trace Element Analysis By Automated Gamma-ray Spectrometry) computer program of Lindstrom and

Korotev (1982).

### *X-ray fluorescence*

Pressed powder pellets were prepared for analysis by wavelength-dispersive X-ray fluorescence. Approximately five grams of powdered sample was mixed with five drops of 2% polyvinyl alcohol solution and pressed at 10 tons with a boric acid backing. A Rigaku model 3064 WD-XRF spectrometer was used to determine concentrations of Ga, Zn, Cu, Ni, Pb, Rb, Sr, and Y at New Mexico Institute of Mining and Technology. X-rays were detected by LiF crystals and measured with a scintillation or gas-flow detector.

Sr and Zn were determined by both methods for all samples except those from the Capitan Mountains (because of a lack of available sample materials). All Sr concentrations plotted in the following figures were determined by XRF except for the Capitan Mountains samples, for which INAA values are used.

### *Fluid inclusion microthermometry*

Doubly-polished thick-sections were prepared from representative fluorite hand samples using standard techniques. Heating and freezing measurements were made on more than 550 fluid inclusions using a Linkham THMS 600 heating/freezing stage. Homogenization temperatures ( $T_h$ ) have an estimated maximum error of  $\pm 2$  °C and melting temperature ( $T_m$ ) measurements are estimated to be accurate

to  $\pm 0.2$  °C as determined by melting point standards. Salinities were calculated using the revised freezing-point depression curve of Bodnar (1992). Microthermometric results are listed in Appendix I.+

#### *Stable isotope mass spectrometry*

A complete description of the procedures used in this study is given in Appendix IV. Inclusion fluids were liberated by invacuo thermal decrepitation of prepared fluorite samples at temperatures of about 600 °C. The extracted waters were collected in microequilibration vessels and cleaned of inclusion-derived CO<sub>2</sub> using an ethylene glycol-dry ice slush. About 20  $\mu$ moles of cleaned CO<sub>2</sub> of known isotopic composition was added to 1-20 mg of fluid inclusion water and equilibrated. The microequilibration vessels were immersed in a water bath at a known temperature of 44-46 °C for a period of 72 hours.

After complete equilibration, CO<sub>2</sub> was removed from the microequilibration vessels and analyzed. The remaining waters were converted to H<sub>2</sub> using the uranium-reduction method of Bigeleisen et al. (1952) and analyzed. All isotope analyses were done on a Finnigan MAT delta-E mass spectrometer using OZTECH gas standards.

Maximum errors were determined by microequilibration and uranium reduction of standard waters and are  $\pm 1.8$  permil for oxygen and  $\pm 5$  permil for hydrogen (Appendix II).  $\delta D$  values have been corrected for memory effects using the

equation of Morse et al. (1993) and are reported as  $\delta D_S$  (see Appendices II and IV). In addition, it was determined, by microequilibration and subsequent uranium reduction of standard waters, that it was necessary to add 4 permil to the  $\delta D_S$  values.

## GEOLOGY AND MINERALIZATION

Descriptions of geology and mineralization for each deposit are given in Table 1. The sampled deposits are hosted by a wide variety of lithologies including pre-Cambrian plutonic and metamorphic rocks, Paleozoic carbonates, sandstones, and shales, and Tertiary plutonic and volcanic rocks. Mineralization occurs predominantly as open space filling and as bedding-replacement in carbonaceous rocks. Fissure veins measuring up to a few meters in width are common in all host lithologies. Syndepositional tectonic activity is indicated by the presence of fluorite-cemented breccias in some deposits.

Sampled veins and replacement deposits are chiefly fluorite and quartz, but may contain calcite, barite, sulfides and oxides. Galena is the most commonly occurring sulfide but pyrite, chalcopyrite, sphalerite, and molybdenite are also found in some deposits. Wulfenite is present in several deposits along the Rio Grande rift, and occurs with molybdenite and vanadinite in the Harding and Cox veins (FL14 and FL15). Fluorite from metallic ore bodies was collected at the Hansonburg district (FL39-FL43),

Table 1.  
Deposit descriptions.

Region/Deposit	Sample number	Deposit style	Host lithology *	Major mineralogy <sup>a</sup>	Latitude deg. min. sec.	Longitude deg. min. sec.	References
Sierra Cuculillo	FL1	vein	pZ limestone	f-bar-cal-qtz	33 23 51	107 36 42	Hartley (1934), Jahns et al (1978), Huskinson (1975), Rothrock et al. (1946)
Hanson Chise	FL5	vein and replacement	pZ limestone	f-bar-cal-qtz	33 16 33	107 34 21	
Socorro area	FL7	vein	pZ siliciclastics	f-bar-qtz	34 04 33	106 48 40	Woodward (1973), McLemore (1980)
Gonzales (east)	FL8	vein	pZ lms/pc granite	f-bar-qtz-grn	34 04 37	106 48 26	
Gonzales (west)	FL9	vein	pc granite	f-bar-qtz-cal-grn-sp-wu	34 11 18	106 59 12	
Lernitar							
Sierra Caballo	FL10	vein	pZ limestone	f-cal-qtz	33 04 57	107 13 35	Hartley (1934), Rothrock et al. (1946), McAnully (1978)
Yellowjacket	FL12	vein	pc granite	f-cal-qtz-cpy	33 04 50	107 14 46	
Independence	FL13	vein	pZ lms/pc granite	f-cal-qtz-cpy	33 01 40	107 14 26	
Marion	FL14	vein	pZ limestone	f-cal-qtz-gr-wu-van	33 02 28	107 12 57	
Hardin	FL15	vein	pZ limestone	f-cal-qtz-gr-wu-van	33 01 20	107 13 07	
Cox	FL16	vein and replacement	pZ limestone	f-qtz-cal	32 49 54	107 15 16	
Nakaya	FL17	vein	pZ limestone	f-qtz-cal	32 48 15	107 16 04	
Esperanza							
Organ Mountains	FL18	vein and replacement	pZ limestone	f-bar-cal-qtz	32 11 40	106 35 51	Rothrock et al. (1946), Gilder (1989), Dunham (1935)
Hiebert	FL19	vein and replacement	pZ limestone	f-bar-cal-qtz	32 11 31	106 35 51	
Grants	FL20	vein	pZ limestone	f-bar-cal-qtz	32 22 01	106 35 39	
Ruby/Hayner							
Fluorite Ridge	FL24	vein	T granodiorite por.	f-qtz	32 23 38	107 42 25	Rothrock et al. (1946), Griswold (1961), McAnully (1978)
Greenleaf	FL25	vein	T monzonite por.	f-qtz-py	32 23 48	107 42 45	
Sadler	FL26	vein	T andesite	f-qtz	32 23 57	107 42 30	
Lucky	FL27	vein	T andesite	f-qtz	32 24 44	107 44 41	
Gratten	FL28	vein	T granodiorite por.	f-qtz	32 24 57	107 44 10	
Green Spar							

\* pc - pre-Cambrian, pZ - Paleozoic, K - Cretaceous, T - Tertiary, lms - limestone, por - porphyry.  
<sup>a</sup> f - fluorite, qtz - quartz, bar - barite, cal - calcite, MnOx - manganese oxides, gn - galena, sp - sphalerite, py - pyrite, cpy - chalcopyrite, wu - wulfenite, van - vanadinite, atag - aragonite, ad - adularia.

Table 1 (continued).  
Deposit descriptions.

Region/Deposit	Sample number	Deposit style	Host lithology *	Major mineralogy <sup>a</sup>	Latitude deg. min. sec.	Longitude deg. min. sec.	References
Lordsburg district							
Antrnas mine	FL29	vein	T thyoilite por.	fl-qtz-cal-MnOx	32 07 40	108 46 40	Elston (1979), Lasky (1938)
Fluorite Group	FL30	vein	K basalt	fl-qtz-cal	32 14 48	108 46 13	
Lone Star	FL31	vein	K/T granodiorite	fl-qtz	32 16 09	108 44 58	
Big Burro Mountains							
Spar Hill	FL32	vein	T thyoilite/PC granite	fl-qtz	32 37 23	108 28 43	Gillerman (1952), Hewitt (1959)
Shrine	FL33	vein	PC granite	fl-qtz-MnOx	32 38 52	108 27 08	
Long Lost Brother	FL34	vein	PC gneiss	fl-qtz-MnOx	32 38 43	108 34 15	
Gila Fluorospas district							
Foster	FL35	vein	T trachitic latite	fl-qtz-bar	33 02 20	108 30 57	Rothrock et al. (1946), Ratte* et al. (1979),
Clum	FL36	vein	T trachitic latite	fl-qtz-bar	33 02 16	108 30 05	McCowan (1993)
Steepie Rock district							
Goat Camp Spring	FL37	vein	T andesite	fl-qtz-py	32 49 43	109 03 20	Elston (1961), Gillerman (1964), Ruff (1994), McLemore (1994)
Hansonburg district							
Ora	FL39	vein and cave filling	PZ limestone	qtz-fl-bar-cal-gn-sp	33 50 13	106 21 54	Kottowski and Steensma (1979),
Ora	FL40	vein and cave filling	PZ limestone	qtz-fl-bar-cal-gn-sp	33 50 13	106 21 54	Putnam (1980)
Ora	FL41	vein and cave filling	PZ limestone	qtz-fl-bar-cal-gn-sp	33 50 13	106 21 54	
Royal Flush	FL42	vein and cave filling	PZ limestone	qtz-fl-bar-cal-gn-sp	33 50 49	106 21 33	
MexTex	FL43	vein and cave filling	PZ limestone	qtz-fl-bar-cal-gn-sp	33 49 44	106 22 10	
Zuni Fluorospas district							
Spruce Hill	FL50	vein	PC granite gneiss	fl-qtz-bar-cal-arag	35 00 59	107 09 05	Rothrock (1946)
Bonita	FL51	vein	PC granite gneiss	fl-qtz-bar-cal-arag	35 04 04	108 00 29	
Capitan Mountains							
	CPU-1	vein	T alkali granite	qtz-fl-ad	33 39 09	105 28 12	Kelley (1971), Allen and McLemore (1991),
	FN	vein	T alkali granite	qtz-fl-ad	33 38 42	105 27 42	Phillips (1990), Phillips et al. (1991)
	CM239	vein	T alkali granite	qtz-fl-ad			
	KS-1	vein	T alkali granite	qtz-fl-ad	33 37 27	105 26 36	
	W3-4	vein	T alkali granite	qtz-f-ad	33 36 19	105 26 36	
	W3-6	vein	T alkali granite	qtz-fl-ad	33 36 19	105 26 36	
	McCoy	vein	T alkali granite	qtz-fl-ad	33 38 29	105 25 29	

\* PC - pre-Cambrian, pZ - Paleozoic, K - Crataceous, T - Tertiary, lms - limestone, por - porphyry.  
<sup>a</sup> fl - fluorite, qtz - quartz, bar - barite, cal - calcite, MnOx - manganese oxides, gn - galena, sp - sphalerite, py - pyrite, cpy - chalcopyrite, wu - wulfenite,  
van - vanadinite, arag - aragonite, ad - adularia.

the Harding and Cox veins (FL14 and FL15), and the Marion Cu mine (FL13). Fluorite samples from the Hayner mine (FL20), the Lordsburg district (FL29-FL31), and the Steeple Rock district (FL37) are from fluorite-quartz-barite zones peripheral to metallic orebodies.

The sampled deposits can be categorized based on the tectonic settings in which they occur. Those occurring within the Rio Grande rift include the Lemitar Mountains, Gonzales prospects, Hansonburg district, Sierra Cuchillo, and Organ Mountains deposits. The Capitan Mountains and Zuni Mountains deposits are spatially associated with the Capitan and Jemez lineaments, respectively. All remaining deposits occur in a region that is dominated by basin and range extensional tectonism. The descriptions of geology and mineralization below are organized by region or district.

#### *Lemitar Mountains Deposits*

The sampled vein in the Lemitar Mountains is hosted by pre-Cambrian granite. Outcrops of a metagabbro stock, mafic dikes and sills, and carbonatite dikes occur near the sampled deposit (Woodward, 1973; McLemore, 1980). Tertiary volcanic rocks are widespread on the western slope of the Lemitar Mountains but only small sporadic occurrences are present on the eastern slope near the fluorite deposits. Multiple episodes of faulting have produced north-south, northeast, and east-west trending fault sets. The sampled

vein is hosted in a northeast-trending fault spatially associated with sub parallel carbonatite dikes. Mineralization consists of quartz, barite, fluorite, galena, sphalerite, and wulfenite.

#### *Gonzales prospect*

Two parallel high-angle faults host fluorite mineralization at the Gonzales prospect. One vein occupies a fault in the western flank of an anticline which is parallel to the fold axis and strikes N15°W (Rothrock, 1946). This fault juxtaposes pre-Cambrian granite against Paleozoic limestone in the downthrown block. Another vein east of the anticline's axis is hosted by Paleozoic carbonaceous siliciclastic rocks. Both veins are comprised of fluorite, barite, and quartz; trace galena is found in the west vein. Silicification of the granite is pervasive for several meters away from the west vein. Argillic alteration is also present within the granite but has not been linked to fluorite mineralization.

#### *Hansonburg district*

Mineralization at Hansonburg is hosted by Paleozoic limestones and is present as open space fillings in fissures, fault breccia, small caves, and as minor replacement of siliciclastic rocks (Kottlowski and Steensma, 1979). The Paleozoic rocks are intruded by monzonite-diorite dikes and sills of Tertiary age. Mineralized bodies



are lenticular and elongate in a north-south direction. They appear to have formed from fluids that were trapped beneath relatively impermeable argillaceous beds. Major phases include barite, fluorite, quartz, calcite, and galena. Numerous Pb, Zn, Cu, and Mo sulfides, oxides, hydroxides, phosphates, and sulfates have also been reported (Taggart et al., 1989).

#### *Sierra Caballo deposits*

Fluorite is hosted by Paleozoic limestones in the eastern slope of the Sierra Caballo and by Paleozoic limestone and pre-Cambrian granite in the western slope (Rothrock, 1946; McAnulty, 1978). Tertiary monzonite porphyry and syenite outcrop in the southern part of the range (near FL16 and FL17) but are absent to the north. North-trending high-angle normal faults, related to the development of the Rio Grande rift, host most of the mineralization.

Two fluorite-bearing assemblages occur in the Sierra Cuchillo (Harley, 1934): fluorite-quartz±barite±calcite±pyrite±chalcopyrite (FL10-FL13 and FL16-FL17), and fluorite-quartz-calcite-galena-vanadinite-molybdenite-wulfenite (FL14 and FL15). All of the deposits occur as fissure veins with only minor wall-rock replacement. The fluorite-galena-vanadinite-molybdenite deposits are found east of the crest of the Sierra Caballo while barren fluorospar deposits are present on the western slope.

### *Organ Mountains deposits*

Fluorospars deposits in the Organ Mountains occur as fissure veins and bedding replacement deposits in Paleozoic limestones. Tertiary monzonite porphyry plutons intrude the Paleozoic sedimentary package in the Organ Mountains. Tertiary andesite, latite, and rhyolite flows and domes are also present in the Organ Mountains (Rothrock, 1946; Dunham, 1935). Mineralization consists of fluorite, barite, quartz, and calcite. Jasperization is common in carbonate rocks near the fluorospars deposits.

One fluorite sample (FL20) was collected from a fluorite-barite vein which occupies a position peripheral to the Organ mining district. Zonation in this district forms a central core of Cu orebodies with successive peripheral zones of Zn, Ag-Pb, and finally fluorite-barite mineralization. The formation of ore deposits in the district appears to be related to the emplacement of an underlying monzonite porphyry stock of the Organ batholith (Dunham, 1935).

### *Sierra Cuchillo Deposits*

Fluorite-bearing deposits in the Sierra Cuchillo occur as skarns, and carbonate-hosted fissure veins and strataform replacement deposits. Paleozoic carbonates and siliciclastic rocks in the Sierra Cuchillo are intruded by numerous monzonite, andesite, and rhyolite dikes, sills, and

stocks of Tertiary age. Extrusive rocks include rhyolite domes and tuffs (Harley, 1934).

Several small fluorite-bearing beryllium skarns are present in the northern part of the range (Jahns et al., 1978). Barren fluorite-quartz-calcite veins and replacement bodies occur in the central and southern parts of the range. Jasperization typically accompanies fluorite mineralization in the carbonaceous rocks. Rhyolite flow domes in the area are typically hydrothermally altered (Harrison, 1986). Fluorite mineralization in the Chise district is hosted by Paleozoic limestones and occurs as epithermal veins and replacement bodies (Huskinson, 1974). Tertiary syenite is present in the Chise district and may have influenced fluorite mineralization.

#### *Capitan Mountains Deposits*

The Tertiary Capitan pluton hosts numerous Th-U-REE-quartz/fluorite veins at its western end (Phillips et al., 1991). Geology of the Capitan Mountains deposits is described by Kelley (1971) and by Allen and McLemore (1991). The pluton is a zoned alkali granite emplaced along the Capitan lineament where it intrudes Permian rocks of the Yeso and San Andres Formations. Differential erosion exposes the granophyric carapace in the western end of the intrusive, an aplitic zone in the center, and the porphyritic granite core of the pluton to the east.

Several small iron skarns are present at the periphery

of the pluton on its western end. The quartz/fluorite veins occur only in the granophyric and aplitic zones where preserved near the top of the pluton at its western end and along its flanks. Mineralization is contained as fissure veins and breccia fillings within the pluton. The veins range from a few centimeters up to several meters in width and can be traced along as much as 300 meters in length (Phillips, 1990). Major mineralogy of the veins includes quartz, fluorite, adularia, and hematite. The fluids responsible for the formation of quartz/fluorite veins in the Capitan mountains have been proposed to be of magmatic origin (Phillips et al., 1991) based on fluid inclusion and stable isotope studies, as well as field observations.

#### *Fluorite Ridge Fluorospar District*

Mineralization at Fluorite Ridge is hosted by a late Cretaceous\early Tertiary granodiorite porphyry containing andesitic and monzonitic phases (Rothrock et al., 1946; Griswold, 1961; McAnulty, 1978). The stock intrudes Paleozoic strata and a thick Tertiary rhyolitic and andesitic volcanic sequence which rests on pre-Cambrian granite. Emplacement of the stock appears to be controlled by a northwest-trending fault zone coincident with the axis of Fluorite Ridge (Griswold, 1961). The youngest igneous rocks in the area are basaltic dikes which cut Miocene (?) conglomerate and are in turn cut by fluorite mineralization (Griswold, 1961). This constrains the age of mineralization

to late Tertiary or younger.

Fluorite and quartz comprise the bulk of the vein material at Fluorite Ridge. Calcite and rare barite occur as trace phases in a few veins. Pyrite has been reported from deep portions of the Sadler vein (FL25) and is the only sulfide known to be present in the district. North-trending fissure veins present within the granodiorite and the overlying volcanic rocks host most of the fluorospar. Vein widths range from a few centimeters up to about six meters and ore shoots generally extend for no more than 30 meters. The deepest workings in the district reveal no appreciable change in vein character to a depth of about 150 meters (Griswold, 1961). Wall-rock replacement is nearly absent and alteration is only weakly developed in the district.

#### *Lordsburg District*

Mineralization in the Lordsburg district was first described by Lasky (1938). The Lordsburg district is in the Pyramid Mountains which are comprised of a late Cretaceous/early Tertiary granodiorite stock and numerous associated quartz latite and felsite dikes which intrude a volcanic pile of basaltic composition. The basaltic sequence contains several thin rhyolite horizons of Cretaceous age, and is intruded by early Cretaceous rhyolite breccia plugs and volcanic necks. The basalt unconformably overlays Pennsylvanian Magdalena limestone. Quartz latite flows, breccias, and necks are the youngest volcanic rocks

in the district. These are overlain, in places, by Quaternary sands and gravels.

Mineralization is contained in numerous east-west and northeast trending high-angle faults. Pre-, syn-, and post-mineral movement is apparent in most areas (Lasky, 1938). A few northwest-trending faults are also present in the district and appear to postdate mineralization. Mineralization at Lordsburg is outwardly zoned with a central copper zone grading into a lead-silver zone and finally into a fluorite zone at the periphery of the district.

Fluorite collected from the Pyramid Mountains is from three fluorite-quartz veins which are present along the southern periphery of the Lordsburg district. One of these is hosted by Cretaceous basalt, another is present in the granodiorite stock, and the third occurs in rhyolite porphyry. Fluorite veins in this area are about one meter in width and can be traced for several hundred meters along strike. No alteration was noted in the basalt but the granodiorite and rhyolite-hosted veins occur in argillized rocks.

#### *Big Burro Mountains Deposits* \*

Sampled fluorospar occurrences in the Big Burro Mountains include the Spar Hill and Shrine mines, and the Long Lost Brother prospect. These deposits are described by Gillerman (1952). Fissure vein deposits in the Big Burro

Mountains occur along northeast-striking faults which cut pre-Cambrian granite of the Burro Mountains batholith and metamorphic rocks of the Bullard Peak Series (Hewitt, 1959). Tertiary rhyolite, andesite, latite, and quartz latite dikes and plugs, and small diorite plutons intrude the pre-Cambrian granite and metamorphic rocks in the vicinity of the fluorospar deposits. At the Shrine mine, Cretaceous (?) andesite porphyry and diabase dikes, and late Cretaceous/early Tertiary monzonite porphyry intrude the Burro Mountains batholith and the Bullard Peak Series metamorphic rocks.

The Long Lost Brother and Spar Hill deposits contain fluorite and finely crystalline quartz. No sulfide or associated metals mineralization is known at these deposits. The Shrine mine deposits, however, are composed of fluorite and quartz with minor pyrite and trace amounts of gold (Gillerman, 1952). Tertiary rhyolite dikes are cut by the east-west striking fissure veins thereby constraining the age of mineralization. Alteration near the veins consists of sericite and quartz.

#### *Gila Fluorospar District*

Fluorite from the Gila fluorospar district was collected from the Foster and Clum mines. These deposits occur as steeply-dipping north-striking fissure veins developed in Tertiary trachytic latite (Rothrock et al., 1946). The typical thickness of this vein is about three

meters and the workings extend to a depth of 160 feet. Fluorite, quartz and fine-grained barite are the only minerals present in the vein. No metallic minerals have been found in the Gila Fluorospars veins although anomalous gold values have been reported by Ratte' (1979). Argillic alteration is present in wall rocks along the veins. Acid-sulfate alteration occurs in the district (McLemore, 1994).

### *Steeple Rock District*

Geology and mineralization in the Steeple Rock district is described by Elston (1961), Gillerman (1964), Ruff (1994), and McLemore (1994). The Steeple Rock district contains four dominant lithologic units which are termed by Elston (1961) as dacite, rhyolite, andesite, and Datil Formation undifferentiated. Except for the rhyolites, which also occur as intrusive masses, all of these rocks form flows, tuffs, and flow breccias. The dacites, rhyolites, and andesites are of upper Cretaceous age (Elston, 1961) and the Datil Formation is grouped as a Tertiary unit.

The Steeple Rock and East Camp faults are steeply-dipping northeast-trending structures which provided strong controls on mineralization. Parallel to these are several less extensive high-angle faults and fractures along which mineralization is localized. Precious metals ore bodies are contained as fissure veins in a zone eight to ten miles along these faults (Gillerman, 1964). The ore bodies are comprised of quartz and pyrite, with minor calcite, barite,



fluorite, chalcopyrite, sphalerite, galena, argentite, tetrahedrite, cerargyrite, gold, and silver. Fluorite sampled from the district is from barren fluorite-quartz veins which occur peripheral to the ore bodies, as is the case at the Lordsburg and Organ districts described above.

Alteration in the Steeple Rock district is described by McLemore (1994). Propylitization, silicification, and argillization of wall rocks is widespread. Additionally, numerous pods of acid-sulfate alteration are present in the district, indicating a predominance of sulfur-rich fluids in the district for at least some of its history.

#### *Zuni Mountains Fluorospa District*

Deposits in the Zuni Mountains fluorospa district occur in the pre-Cambrian Zuni Mountains granite and granitic gneiss (Rothrock et al., 1946). These rocks form the core of the Zuni Mountains and are deformed into a northwest-trending arch. Paleozoic sediments flank the granite core, dipping away from the mountains on the northern and southern sides. Small Quaternary basalt flows and cinder cones are numerous in the district. No other volcanic rocks occur near the fluorospa deposits.

The fluorospa veins occupy northwest-trending steeply-dipping fissures. Open space filling is the dominant style of mineralization, with only minor wall rock replacement. Vein mineralogy includes fluorite and minor barite, calcite, aragonite, and pyrite. Phyllic and argillic alteration

occur within the host granite. Red iron staining is common near the fluorospar veins. No metallic mineral deposits are known to be associated with fluorite mineralization in the Zuni Mountains.

## RESULTS AND DISCUSSION

### *Fluid inclusions*

The fluorite samples used in this study are typically fluid inclusion rich, containing mainly two phase (L+V) water-rich inclusions. Most occur along through-going planes and are therefore classified as secondary. Primary inclusions were also identified in most samples. A small number of one phase liquid and one phase vapor inclusions were found in a few samples and are likely the result of necking (Roedder, 1984). Neither visible CO<sub>2</sub> nor daughter minerals were observed in any fluid inclusions.

The criteria used for the classification of primary inclusions were adopted from Roedder (1984). The most relevant criteria in this study was isolation of single inclusions or small arrays from other inclusions by at least five times the longest primary inclusion dimension. Although some primary inclusions have irregular or smooth and rounded shapes, they typically occupy negative crystal shapes. However, a negative crystal morphology was not assumed to be exclusive to primary inclusions. The average dimensions of measured primary inclusions are 5 - 30 micrometers with some as large as 60 micrometers. In some

samples, inclusions occurring along growth planes parallel to crystal faces were tentatively identified as primary. Occluded solids are present adjacent to the fluid inclusions along many of these planes further establishing their origin as primary. However, because of their small size, microthermometric analysis of these inclusions was not possible.

In most samples, multiple generations of secondary inclusions are evidenced by the crosscutting relationships of numerous secondary planes and by the presence of several secondary morphologies. The dimensions of secondary fluid inclusions range from less than one micrometers up to hundreds of micrometers. Because of the abundance of planes of secondary inclusions in most samples, pseudosecondary inclusions were tentatively identified in only a few samples. However, as is discussed below, many inclusions classified as secondary probably originated from the same fluids responsible for forming primary inclusions.

Microthermometric data for fluorite from the Capitan Mountains was obtained from Phillips (1990) and data for Hansonburg fluorite is from Putnam (1980). Microthermometry was performed by the author on all other samples. No pressure corrections have been applied to the Th data. Therefore, homogenization temperatures represent minimum trapping temperatures. Results from this study are listed in Appendix I.

With the exceptions of inclusions in the Capitan

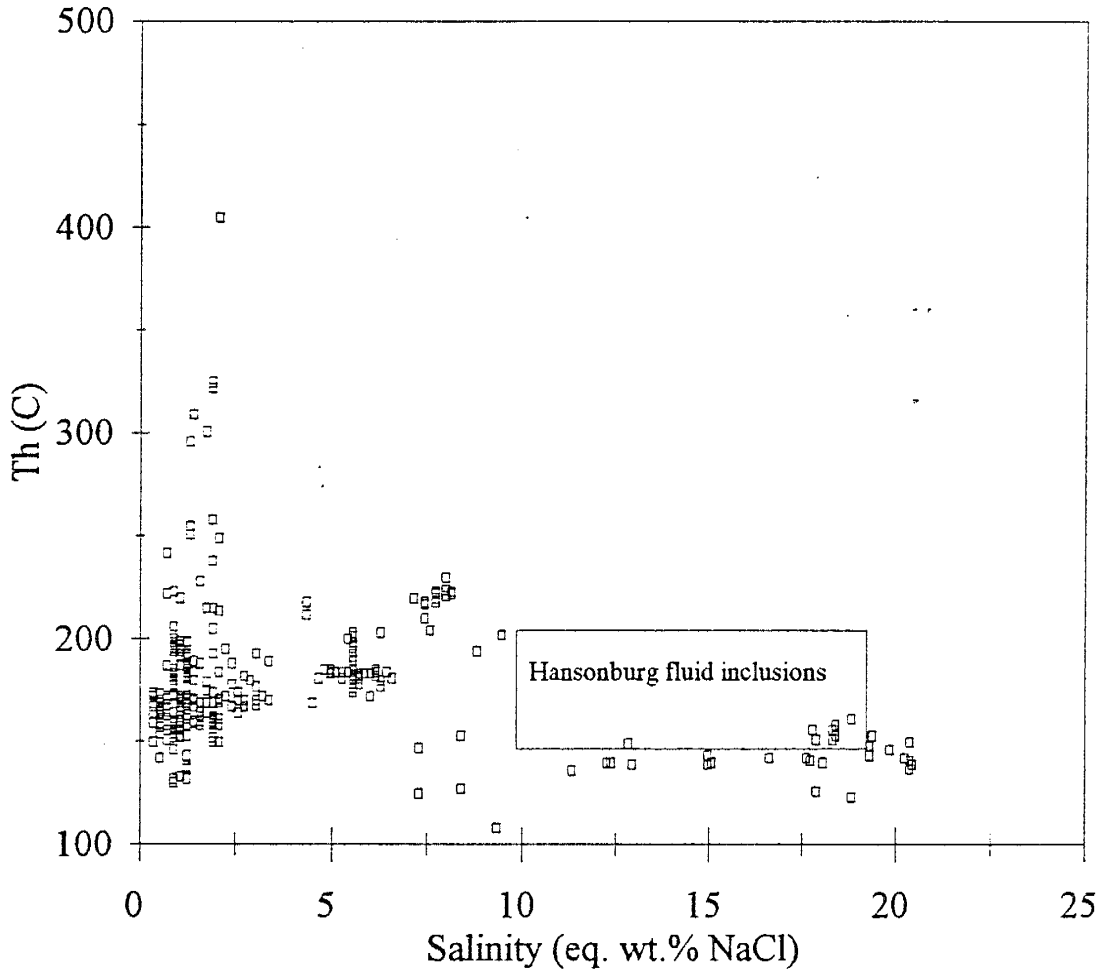
Mountains samples, nearly all primary inclusions homogenize between 100 °C and about 240 °C and have salinities less than 21 eq. wt.% NaCl (Figure 2). The majority of samples contain primary fluid inclusions with salinities less than about 8 eq. wt.% NaCl. Below this value, Th and salinity tend to co-vary whereas fluid inclusions with salinities higher than this homogenize at relatively low temperatures. This break in the data set separates high salinity deposits in the Sierra Caballo (FL14-FL15), the Zuni Mountains (FL50-FL51), and the Hansonburg district (FL39-FL43) from all other sampled deposits.

Apart from the Capitan Mountains samples, the highest homogenization temperatures are from the Hanson deposit (FL1) in the Sierra Cuchillo. Liquid/vapor ratios of primary inclusions in this sample are highly variable. This may be indicative of boiling during fluorite deposition. Excess vapor in fluid inclusions, derived from heterogeneous trapping of liquid and vapor phases during boiling, yields homogenization temperatures which do not represent minimum trapping temperatures (Roedder, 1984).

Fluid inclusions in fluorite from the Capitan Mountains are unique among the data set. They contain as many as eight daughter minerals including halite, sylvite, anhydrite, adularia, and several opaque phases. They homogenize at temperatures as high as 600 °C and have salinities as high as 80 eq. wt.% NaCl. The Capitan inclusions are dominated by magmatic fluids with some

Figure 2. Variation diagram plotting homogenization temperature against salinity. Data from all measured primary inclusions are plotted. Data from Hansonburg is from Putnam (1980). High salinity inclusions are present in the Zuni Mountains fluorites and in the Harding and Cox veins in the eastern slope of the Sierra Caballo. Most deposits contain low salinity inclusions. The Gonzales and Lemitar samples contain primary fluid inclusions with moderate salinities around 5-7 eq. wt.% NaCl. The large range in Th among the low salinity deposits is due largely to boiling at the Hanson deposit in the Sierra Cuchillo.

### Th vs Salinity



potential for mixed meteoric fluids in the inclusions which exhibit the lowest salinities (Phillips, 1990).

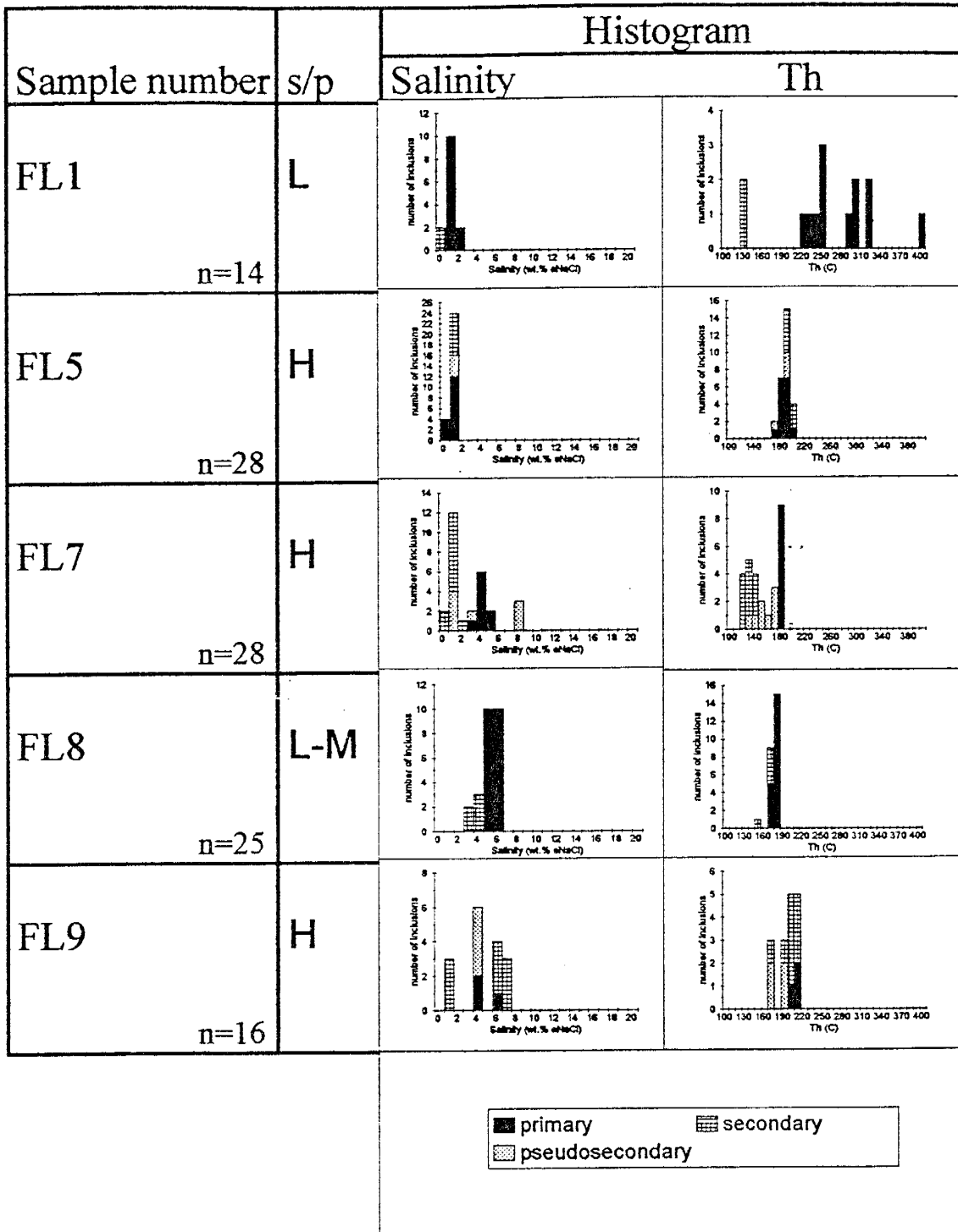
### *Stable Isotopes*

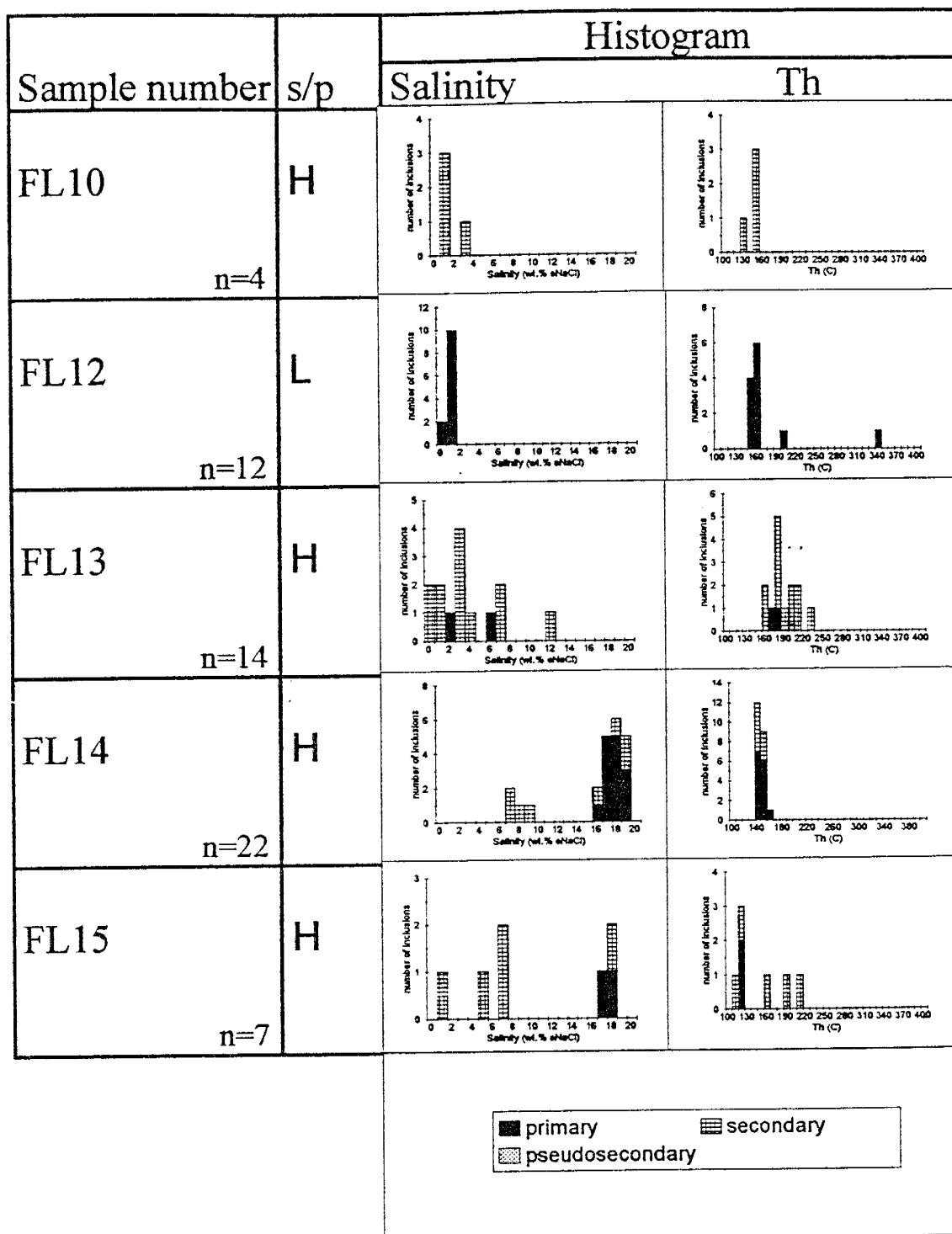
In order to estimate the isotopic compositions of the fluids responsible for fluorite deposition,  $\delta D$  and  $\delta^{18}O$  compositions of inclusion fluids in fluorite separates were measured. Because fluorite is neither oxygen- nor hydrogen-bearing, any post-entrapment fluid-mineral isotope exchange is unlikely. Therefore, the isotopic values of primary inclusion fluids should represent those of the mineralizing solutions. However, where secondary inclusions are abundant and of different isotopic compositions than primary inclusions, they will mask the isotopic compositions of the mineralizing solutions.

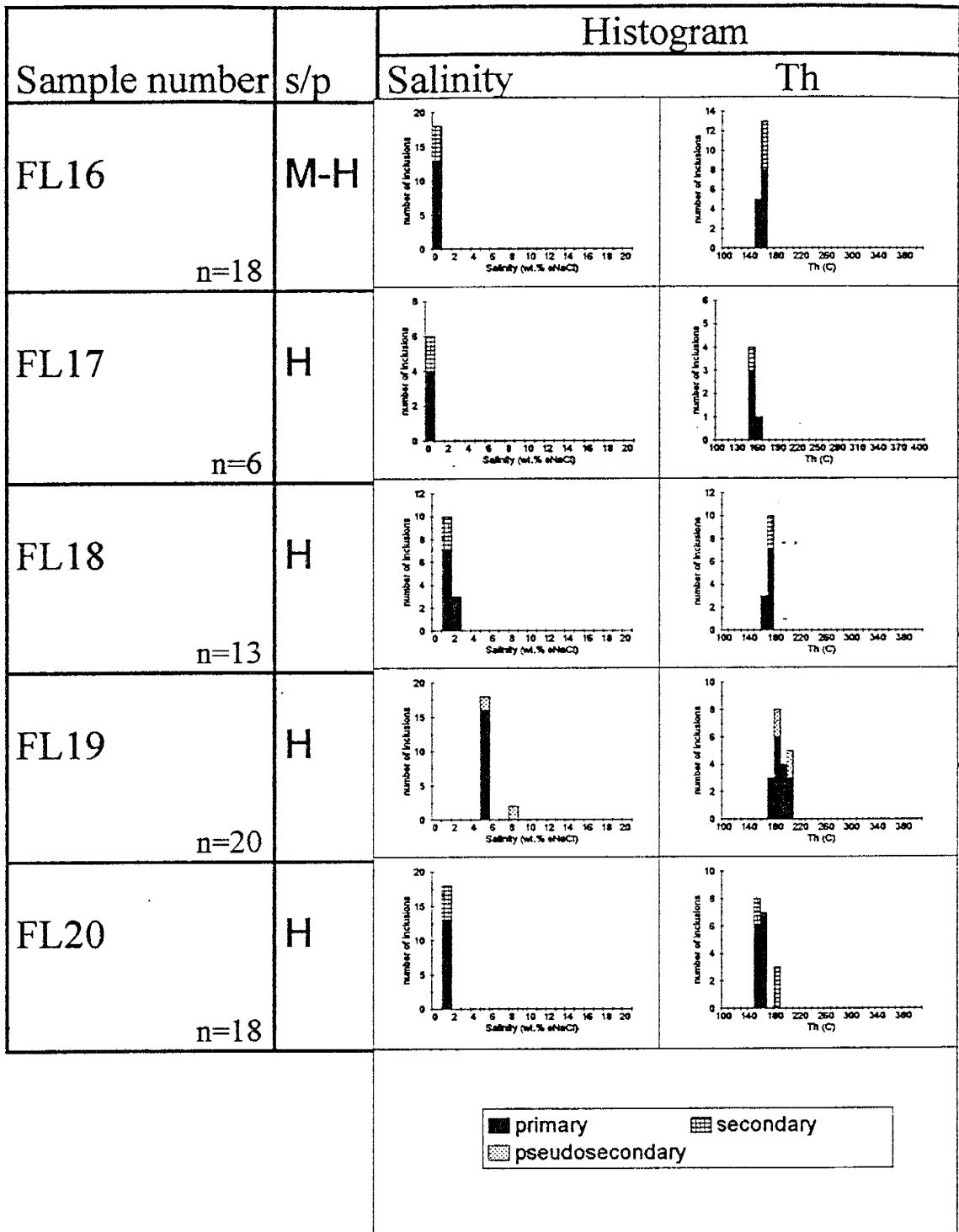
Because the inclusion fluids were liberated by bulk thermal decrepitation of samples containing numerous inclusion generations, the measured values represent the total of all inclusion fluids released from any given sample (Figure 3; Appendix II). In order to assess how closely the measured values approximate the actual compositions of the mineralizing fluids, microthermometric and volume comparisons of all fluid inclusion generations in each sample were made. The overall ratio of secondary to primary inclusion volume was roughly estimated as low, medium, or high in each sample and is

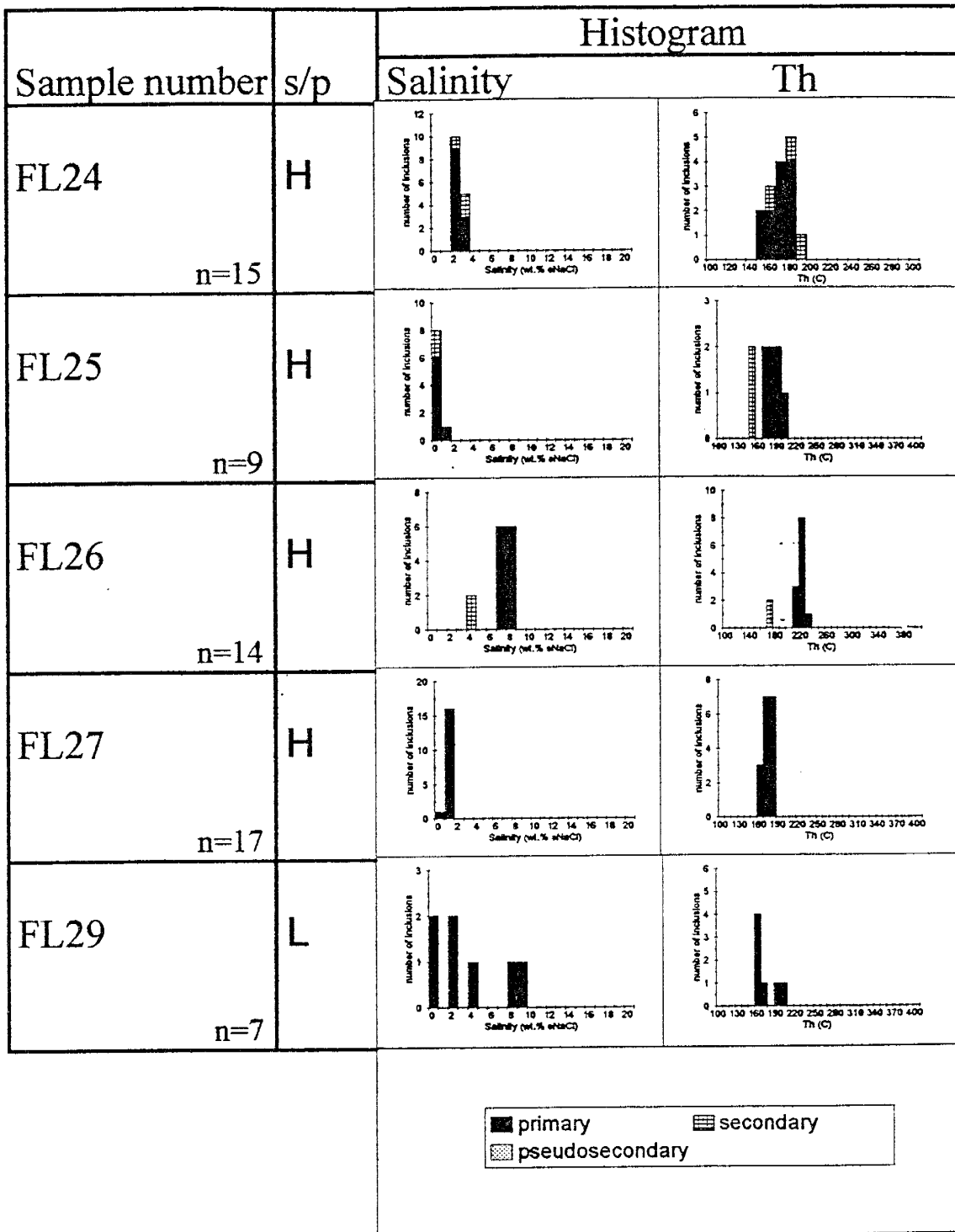
Figure 3. Histograms of primary, pseudosecondary, and secondary inclusions. Visual estimations of the relative amounts of secondary and primary inclusion fluids are given (s/p); L - large, M - medium, S - small. The x-axis scales are uniform among the deposits allowing for easy comparison. Th and salinity ranges tend to be small; however, several deposits do contain fairly large ranges. Th and salinity ranges among the various fluid inclusion generations in individual samples commonly overlap.











Sample number	s/p	Histogram	
		Salinity	Th
FL30 n=11	H		
FL31 n=17	H		
FL32 n=8	M-H		
FL33 n=17	M-H		
FL34 n=18	H		

primary
  secondary  
 pseudosecondary

Sample number	s/p	Histogram	
		Salinity	Th
FL35 n=12	H		
FL36 n=5	L		
FL37 n=19	H		
FL50 n=17	L-M		
FL51 n=17	L		

primary
  secondary  
 pseudosecondary

reported as "s/p" in Figure 3. Salinity and Th comparisons of primary, secondary, and pseudosecondary inclusions are also given in the form of histograms for each sample.

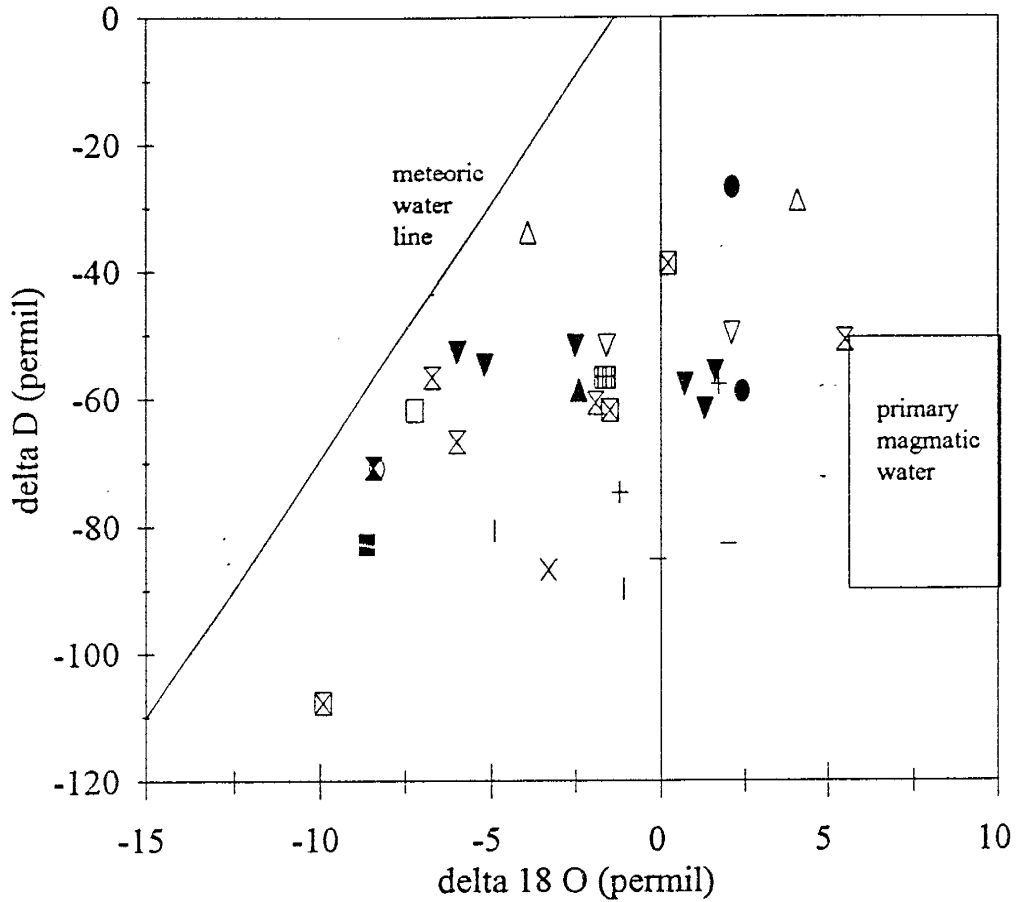
The impact of secondary fluid inclusions on measured  $\delta D$  and  $\delta^{18}O$  is dependent on the relative volumes of secondary and primary inclusion fluids and the isotopic compositions of each. Because it has not been possible to measure isotopic compositions of single inclusion generations, the assumption has been made that inclusion generations which yield similar microthermometric data also contain fluids with similar isotopic compositions. If this assumption holds, then in samples where microthermometric results are similar for all inclusion generations, the ratio of primary to secondary inclusions is insignificant because all contained fluids should have the same isotopic compositions. But in cases where primary and secondary inclusions homogenize at different temperatures and/or are of different salinities, it cannot be assumed that the isotopic compositions are the same for each generation. In such a case, the measured isotopic composition will represent the volume-dominant fluid inclusion generation.

For most samples, although they are dominated by apparently secondary inclusions, all fluid inclusion generations within that sample formed under similar temperature and salinity conditions. Given that, it is not unreasonable to expect that most inclusion generations were formed from the mineralizing fluids. Thus, the isotopic

Figure 4. Variation diagram plotting  $\delta D$  against  $\delta^{18}O$  of inclusion fluids. All samples plot to the right of the meteoric water line. Inclusion fluids from several districts, including Fluorite Ridge, Sierra Caballo, and Lordsburg, plot in horizontal trends with variable  $\delta^{18}O$  but constant  $\delta D$  (within error).



## delta D vs. delta 18 O



■ Hanson	□ Chise	● Gonzales	○ Lemitar
▼ Caballo	▽ Bishop Cap	✕ Organ	⊗ Fluorite Ridge
▲ Lordsburg	△ Animas	+ Big Burro	⊞ Gila
× Steeple Rock	⊠ Hansonburg	Zuni	- Capitan

heavy fluids, possibly of magmatic, metamorphic, or exchanged meteoric origin, cannot be ruled out.

A more plausible explanation calls on variably-exchanged meteoric waters as the mineralizing fluids. This interpretation is supported by the presence of horizontal trends in the data from several districts including Fluorite Ridge, the Sierra Caballo, and the Lordsburg district (Figure 4). Horizontal trends such as these can result from variable  $^{18}\text{O}$  shifts away from the meteoric water line as water/rock oxygen exchange proceeds (Criss and Taylor, 1986). As heated meteoric fluids migrate, they gradually trend toward isotopic equilibrium with the rocks through which they flow. Because rocks contain heavy oxygen relative to meteoric waters, and because water/mineral fractionation factors are small at elevated temperatures, meteoric waters become heavier as they migrate through rock reservoirs. Hydrogen exchange may also occur through this process but shifting waters to higher  $\delta\text{D}$  values requires much more water/rock exchange. This is because, unlike water, rocks contain very small amounts of hydrogen and are therefore inefficient at shifting  $\delta\text{D}$  values of waters. Mixing of heavier waters with unexchanged meteoric waters could also result in the observed distribution of data. However, this would require that both end member fluid components had similar  $\delta\text{D}$  values, since horizontal trends are present. Therefore, it seems unlikely that mixing of two originally unrelated fluids was important in fluorite

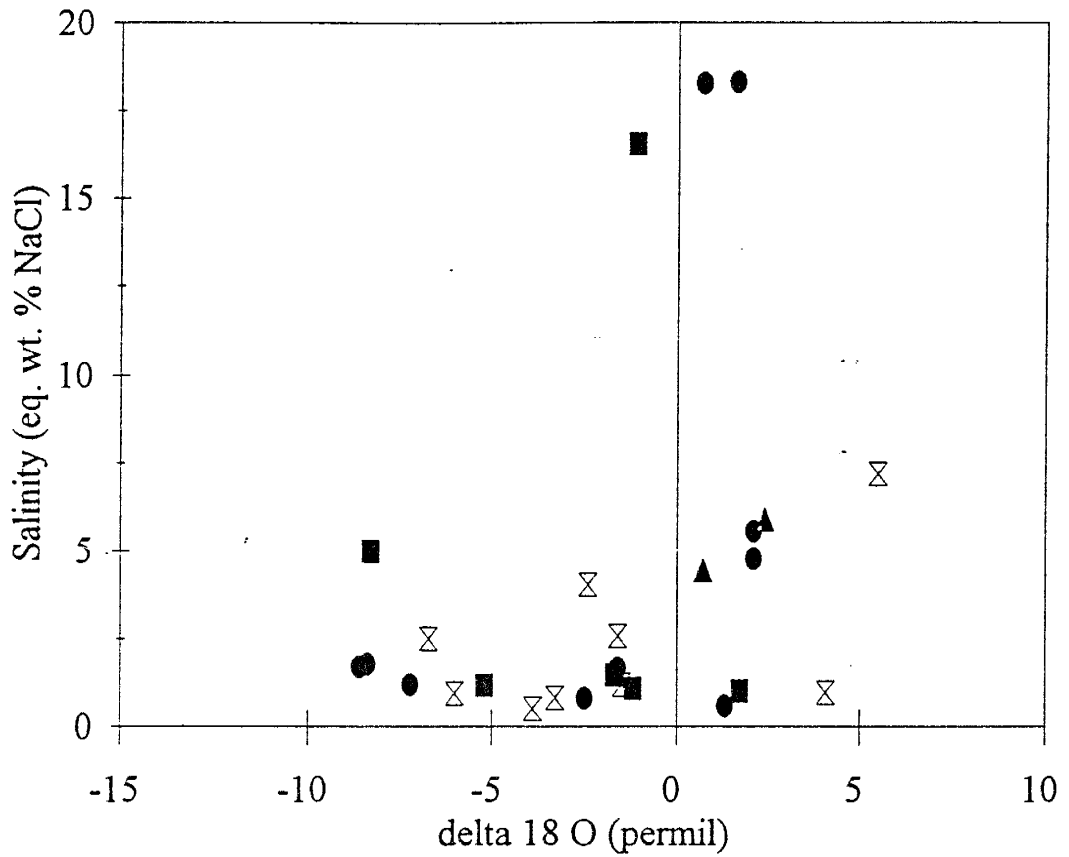
precipitation.

Non-horizontal trends are only present in the data sets from the Hansonburg district, the Gonzales prospects, and the Big Burro Mountains. Because these trends do not project back to reasonable values for meteoric waters, it is difficult to explain these trends by involving differing amounts of unexchanged meteoric waters, contained in secondary inclusions, among deposits in a given region. Several other explanations are possible. Secondary inclusions in these samples may have originated from fluids which were not unexchanged meteoric fluids and were unrelated to the mineralizing solutions. A second explanation is that the individual deposits in these regions formed at different times from exchanged meteoric waters with different initial isotopic compositions. A third alternative is mixing of two exchanged meteoric waters with different isotopic compositions. Microthermometric comparisons of fluid inclusions in these samples do not strongly support any of these interpretations. Therefore, more detailed studies in these regions would be necessary to adequately address this problem.

A weak positive correlation exists between salinity and  $\delta^{18}\text{O}$  (Figure 5). As is discussed above, shifting the  $\delta^{18}\text{O}$  of a meteoric water toward higher values requires that water/rock ratios become progressively smaller as that water migrates through a rock reservoir. During this migration, one might also expect the concentration of solutes to

Figure 5. Variation diagram plotting salinity versus  $\delta^{18}\text{O}$  diagram. A weak positive correlation exists between  $\delta^{18}\text{O}$  and salinity. This would be expected if variably-exchanged meteoric waters were responsible for fluorite deposition.

## Salinity (avg primary) vs delta 18 O



- sediment hosted
- granite hosted
- ▲ granite/sediment hosted
- ⊠ other igneous hosts

increase as a fixed volume of water interacts with more and more rocks. Therefore, this relationship provides further support to the interpretation that the mineralizing solutions in most of the hydrothermal systems were variably-exchanged meteoric waters.

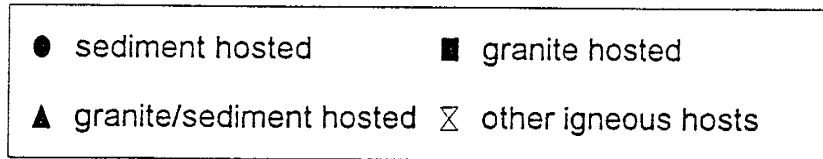
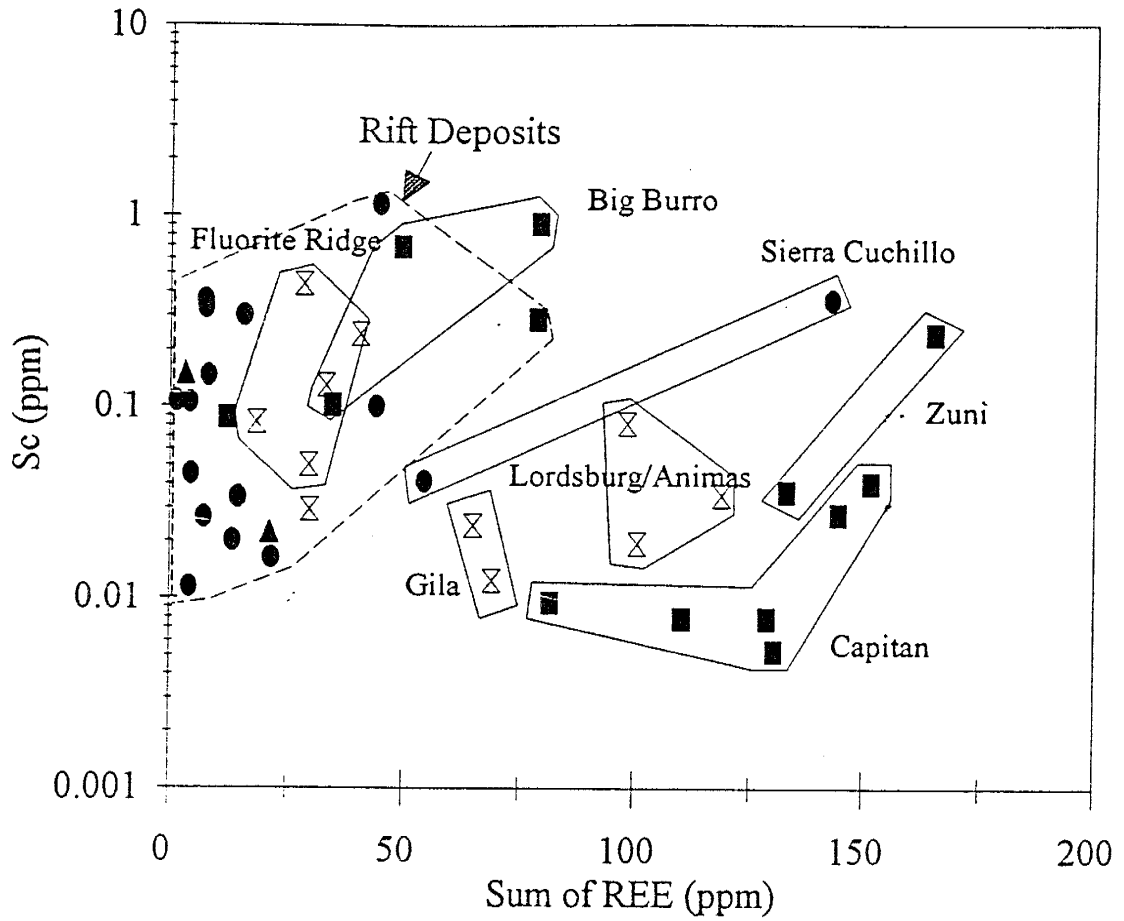
#### *Trace and rare earth elements*

Concentrations of 29 elements determined by INAA and XRF are listed in appendix III. Trace and rare earth elements were detected in all fluorite samples and ranged in concentration from hundredths to tens of parts per million. Cluster analysis as well as visual inspection of numerous variation diagrams was used to search for populations in which fluorite samples have similar compositions.

In a plot of Sc versus  $\Sigma$ REE concentration (Figure 6) samples from each district outside the Rio Grande rift tend to plot together in narrow ranges relative to the overall distribution of data from all districts. Samples from all districts within the Rio Grande rift tend to plot together and can not be separated according to district. Host rock influences on fluorite composition were first established by Fleischer (1969) in a compilation of numerous studies of fluorite deposits occurring in a wide variety of geologic environments. Data from the present study reveal that sediment-hosted fluorites tend to have low  $\Sigma$ REE concentrations relative to fluorite hosted by igneous rocks. Furthermore, limestone-hosted deposits which are spatially

Figure 6. Variation diagram plotting Sc against  $\Sigma$ REE contents of fluorite. igneous-hosted deposits plotted as squares; sediment-hosted deposits plotted as circles; juxtaposed limestone/granite-hosted deposits plotted as triangles. Sedimentary host lithologies contain low  $\Sigma$ REE abundances relative to igneous-hosted deposits. The four sediment-hosted fluorites with anomalously high  $\Sigma$ REE contents are spatially associated with Tertiary igneous rocks. Little overlap occurs among the sampled districts.

### Sc vs Sum of REE





associated with Tertiary intrusive rocks contain fluorite with high  $\Sigma$ REE concentrations relative to all other sediment-hosted fluorites. These include samples from the Sierra Cuchillo (FL1 and FL5) and from the southern Sierra Caballo (FL16 and FL17).

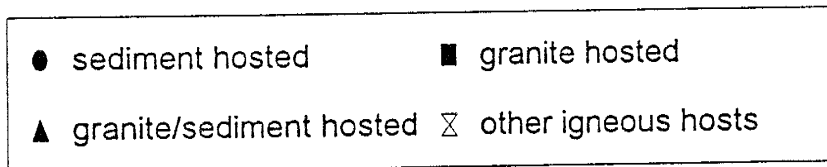
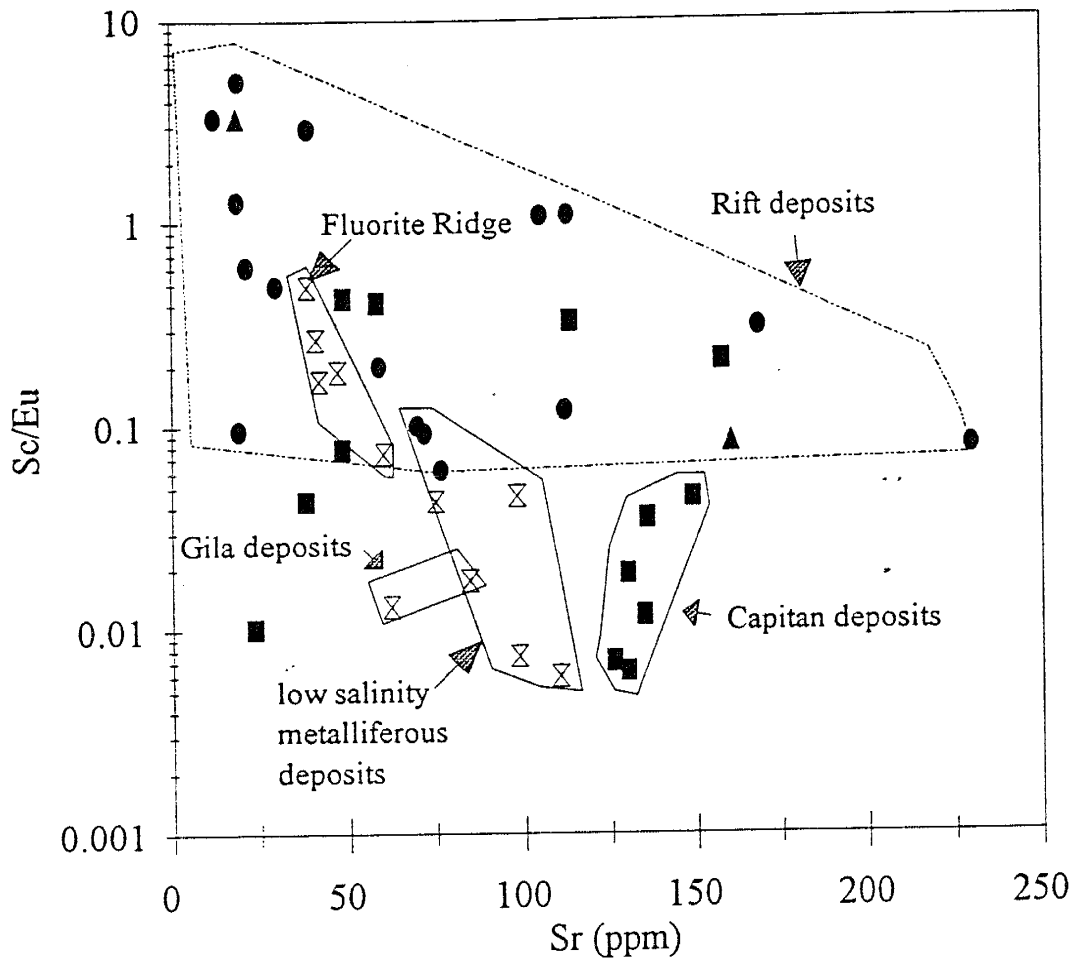
The Lordsburg samples (FL29-FL31) also show evidence of controls on fluorite composition from sources other than the immediate host rocks. Although each sampled deposit in this region is hosted by a separate lithology (rhyolite, basalt, and granodiorite), they tend to have similar compositions. The same applies to the Fluorite Ridge samples (FL24-FL28) which are hosted by granodiorite, monzonite, or andesite. Separate granodiorite stocks, which are the likely sources of Sc and the REE, underlay both districts and host some fluorite deposits.

Lithologic controls are also apparent in a plot of Sc/Eu ratio versus Sr concentration (Figure 7). Igneous-hosted fluorite tends to have lower Sc/Eu ratios than does fluorite which occurs in sedimentary environments. Where the host rocks are igneous, Sc/Eu ratios and Sr contents also tend to be similar among fluorites from the same district. However, sediment-hosted fluorites show large inter- and intra-district variations in Sr concentration and Sc/Eu ratio.

Figure 7 is quite interesting because it defines a geochemical signature indicative of fluorite associated with base and precious metals mineralization. When plotted

Figure 7. Variation diagram plotting Sc/Eu ratio against Sr concentration of fluorite. igneous-hosted deposits plotted as squares; sediment-hosted deposits plotted as circles; juxtaposed limestone/granite-hosted deposits plotted as triangles. All Sr concentrations determined by XRF except for the Capitan Mountains samples for which INAA values are used. Sediment-hosted fluorite tends to have high Sc/Eu ratios relative to igneous hosted fluorite. Fluorite from all sampled low salinity metalliferous deposits plots together in a small field regardless of host lithology. Fluorite from the Gila Fluorospar district plots near the box associated with low salinity base and precious metals mineralization. High salinity metalliferous deposits occupy nearly the entire range defined by fluorite from the Rio Grande rift.

## Sc/Eu vs Sr



against Sr, the Sc/Eu ratio constrains all low salinity metalliferous deposits in one small field. High salinity metalliferous deposits occupy a broad range and are indistinguishable from barren deposits. The fact that all low salinity metalliferous deposits plot together, regardless of host lithology, indicates the importance of compositional influences other than host lithology. These influences may be the Tertiary intrusive rocks which are present in the districts which contain low salinity base and/or precious metals mineralization.

Rather than presenting the standard chondrite-normalized REE profiles, several parameters which represent these patterns are listed below (Table 2). The REE data from all fluorite samples are normalized to chondritic meteorites (Nakamura, 1974) and is summarized in Figures 8 and 9 (Chondrite-normalized parameters are subscripted with "n"). In addition to the abundance of rare earth elements ( $\Sigma$ REE), the (La/Yb)<sub>n</sub> ratio, (Tb/Yb)<sub>n</sub> ratio, and sign and magnitude of europium anomaly differentiate fluorite deposits according to host lithology. These parameters tend to be similar among fluorites from separate districts with similar host lithologies. When combined in scatter plots, these parameters tend to separate sediment-hosted fluorites, granite-hosted fluorites, and fluorites hosted by other igneous rocks.

Granite-hosted fluorites tend to have high REE concentrations, low (La/Yb)<sub>n</sub> ratios ( $\leq 1$ ), low (Tb/Yb)<sub>n</sub>

Table 2. Criteria used for comparing REE profiles.

Total REE = La+Ce+Nd+Sm+Eu+Tb+Yb+Lu (ppm).

La/Yb (n) and Tb/Yb (n) calculated from chondrite-normalized values.

Europium anomaly characterized as positive if  $Eu/Eu^* > 1$  and negative if  $Eu/Eu^* < 1$ .

sample number	total REE (ppm)	La/Yb (n)	Tb/Yb (n)	Eu/Eu*
FL1	143	1.6	1.11	0.6
FL5	54.68	12.31	1.68	0.95
FL7	7.42	6.6	1.61	0.43
FL8	21.38	1.84	1.37	0.42
FL9	12.45	0.82	1.07	0.41
FL10	4.34	3.55	1.52	0.62
FL12	78.75	2.28	1.01	0.81
FL13	3.28	3.23	1.64	0.56
FL14	4.5	19.69	5.91	0.38
FL15	1.43	9.25	4.77	0.38
FL16	44.81	6.31	0.97	0.69
FL17	44.11	4.88	1.98	0.54
FL18	7.73	1.03	2.21	0.65
FL19	14.81	3.29	2.93	0.68
FL20	13.78	20.53	3.48	0.93
FL24	40.66	2.38	2.09	0.92
FL25	18.55	3.92	1.87	0.75
FL26	29.6	5.3	2.26	0.98
FL27	33.34	3.29	1.4	0.84
FL28	28.28	1.05	1.3	0.7
FL29	100.81	3.55	3.39	0.65
FL30	98.47	16.38	3.34	1.13
FL31	118.76	4.22	3.14	1.38
FL32	79.29	0.77	0.95	0.76
FL33	34.67	1.01	1.37	0.8
FL34	49.69	0.17	0.93	0.6
FL35	69.08	404.09	11.93	2
FL36	65.1	7.91	2.77	1.27
FL37	29.8	7.09	3.25	0.97
FL39	15.85	0.9	4.2	0.63
FL40	8.22	1.77	2.89	0.6
FL41	4.31	2	2.83	0.54
FL42	21.78	8.97	1.8	0.54
FL43	7.6	2.78	1.96	0.5
FL50	133.15	0.34	1.53	0.33
FL51	165.24	0.34	1.06	0.55
CM239	110.35	0.81	0.62	0.25
CPU-1	81.83	0.33	0.61	0.17
FN	151.62	0.4	0.78	0.14
KS-1	117.39	0.34	0.78	0.21
McCory	128.94	0.43	0.89	0.18
W3-4	130.45	0.46	0.81	0.16
W3-6	144.57	0.8	0.83	0.17

Figure 8. Variation diagram plotting  $(La/Yb)_n$  versus  $(Eu/Eu^*)_n$ . Subscripted "n" denotes chondrite normalization. Granite-hosted fluorites tend to have low  $(La/Yb)_n$  ratios. Sediment- and other igneous-hosted fluorites have more variable  $(La/Yb)_n$  ratios.  $(Eu/Eu^*)_n$  represents a chondrite normalized europium anomaly. Values greater than one are considered positive while those less than one are considered negative europium anomalies.

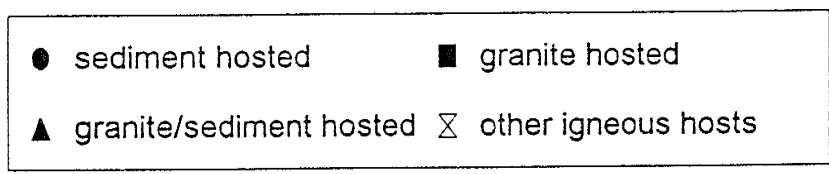
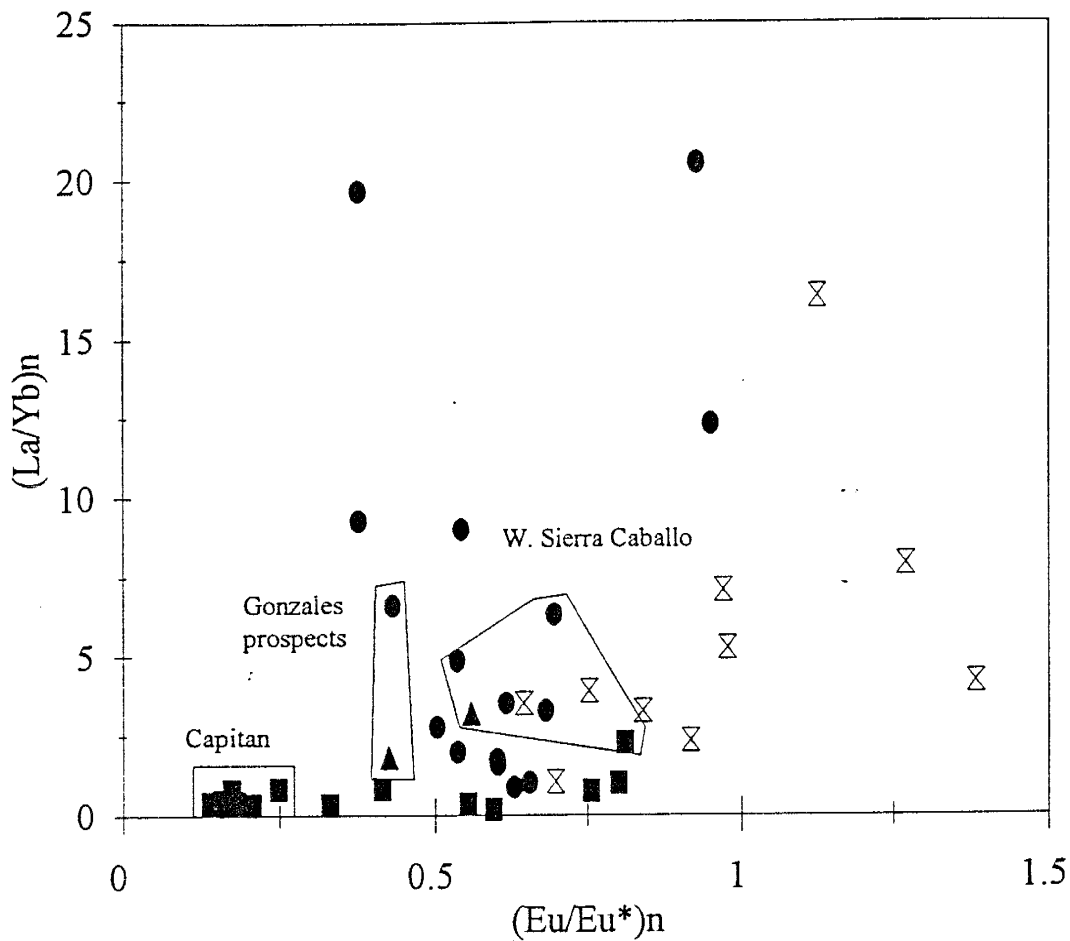
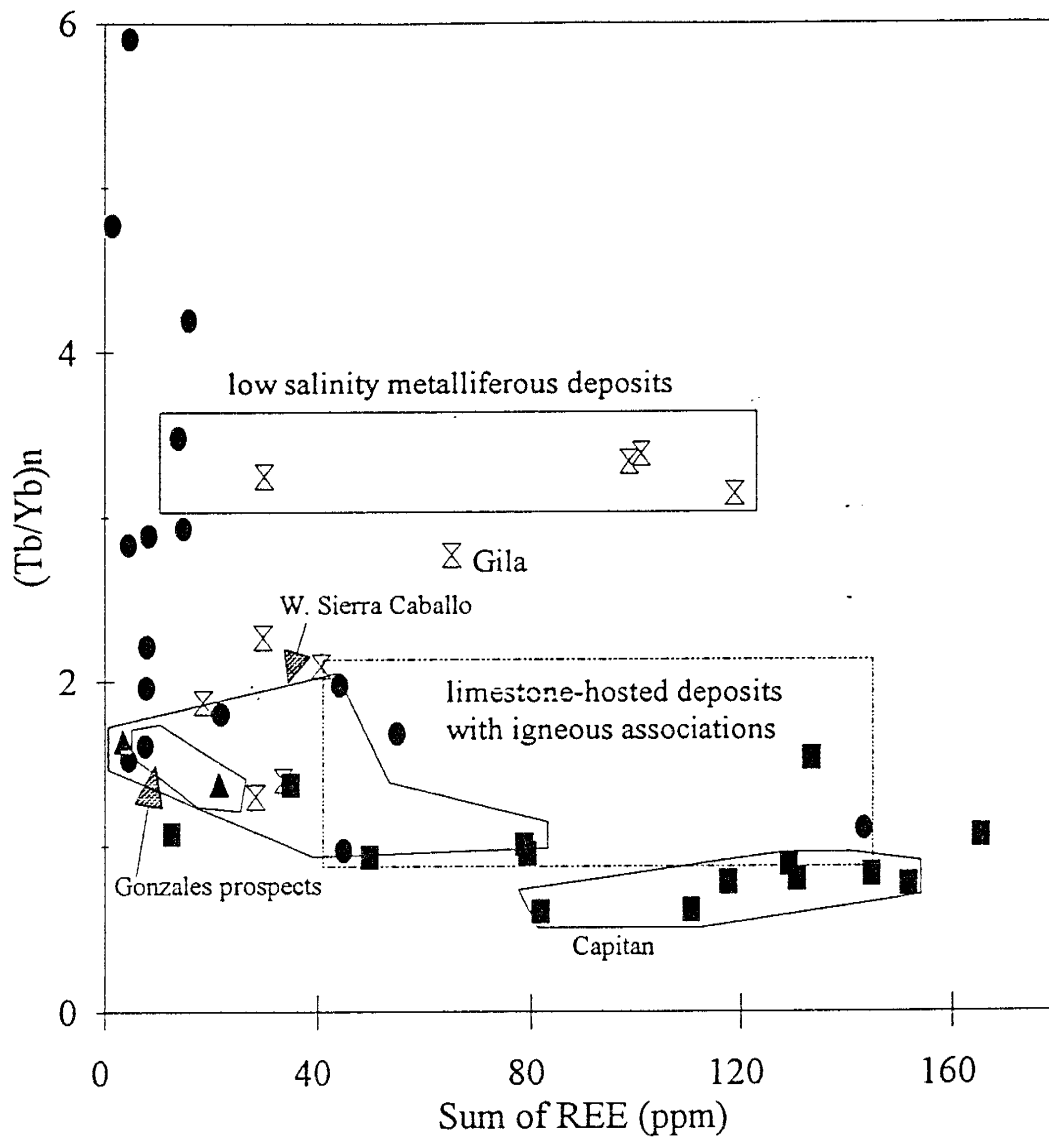
$(La/Yb)_n$  vs  $(Eu/Eu^*)_n$ 

Figure 9. Variation diagram plotting (Tb/Yb)<sub>n</sub> versus Sum of REE. Granite-hosted deposits tend to have low (Tb/Yb)<sub>n</sub> ratios and high  $\Sigma$ REE abundances. Sediment-hosted fluorite has low  $\Sigma$ REE abundance and variable (Tb/Yb)<sub>n</sub> ratios. Fluorite hosted by non-granite igneous rocks tends to plot between the two fields defined by granite- and sediment-hosted fluorite. All fluorite associated with low salinity metalliferous mineralization has (Tb/Yb)<sub>n</sub> ratios between 3.1 and 3.5.



(Tb/Yb)<sub>n</sub> vs Sum of REE

ratios ( $< 1.53$ ), and negative europium anomalies (0.14-0.8). Fluorite hosted by volcanic rocks yields profiles that show moderate REE concentrations,  $(La/Yb)_n$  values between 0.8 and 404,  $(Tb/Yb)_n$  ratios between 0.9 and 11.9, and small negative, positive, or negligible europium anomalies (0.65-2.0). Most of the sediment-hosted fluorites have low to moderate REE abundances,  $(La/Yb)_n$  values between 1.0 and 20.5,  $(Tb/Yb)_n$  ratios between 1.0 and 5.9, and negative europium anomalies (0.38-0.95).

Careful examination of the REE data from fluorite within individual districts reveals more subtle features in sediment-hosted fluorite from deposits associated with igneous rocks. For example, fluorite from the juxtaposed limestone/granite-hosted vein at the Gonzales prospects has a higher  $\Sigma REE$  abundance, and smaller  $(La/Yb)_n$  and  $(Tb/Yb)_n$  ratios than does the sediment-hosted vein at that location. In the western Sierra Caballo samples, two REE populations can be discerned. Three deposits in this region contain fluorite with high  $\Sigma REE$  abundances relative to the other two. One of the fluorites with high  $\Sigma REE$  is granite-hosted and the other two are from deposits associated with Tertiary syenite. Fluorite from the Hanson deposit (FL1), although limestone-hosted, also has  $La/Yb$  and  $Tb/Yb$  ratios which are very similar to those of granite-hosted deposits.

Mineralogical variation among the deposits could not generally be correlated with the observed distribution of Sc and  $\Sigma REE$ ; however, the presence of baestnasite and other

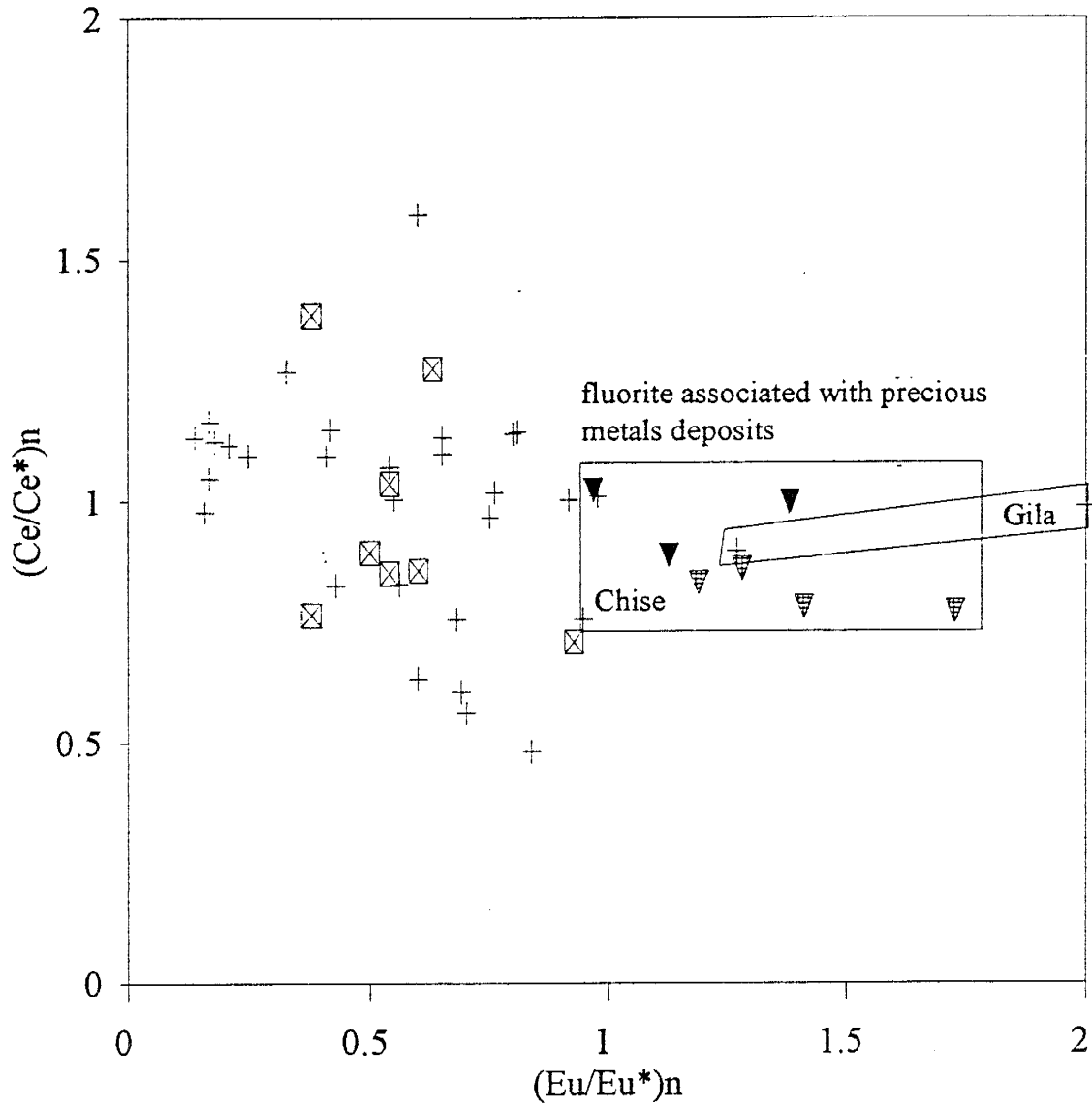
REE phases in the Lemitar Mountains deposits (McLemore, 1980) may explain the low  $\Sigma$ REE abundance in the granite-hosted fluorite sample from that region.

All fluorites associated with low salinity metalliferous mineralization have (Tb/Yb)<sub>n</sub> ratios between 3.1 and 3.5. This is a very small range relative to the total range for all data. The fact that this signature exists strongly suggests that processes which were important for the deposition of base and precious metals also controlled REE fractionation in fluorite from these deposits.

Eppinger (1988) and Eppinger and Closs (1990) in a similar study, noted that fluorite associated with epithermal precious metals veins has a distinctive signature which involves Eu and Ce anomalies (Eu/Eu\* and Ce/Ce\*). Data from this study also differentiates precious metals deposits using these parameters (Figure 10). In addition, fluorite from the Organ Mountains which is peripheral to the low salinity Cu, Zn, and Pb-Ag orebodies in the Stevenson-Bennett district plots adjacent to fluorite associated with precious metals.

Perusal of the available literature (Constantopoulos, 1988; Ekambaram et al., 1986; Strong et al., 1984; Gilder, 1989) indicates that positive europium anomalies in fluorite are rare in other regions as well. However, barren fluorites from south-central Idaho do contain positive europium anomalies (Constantopoulos, 1988). It is

Figure 10. Variation diagram plotting  $(Ce/Ce^*)_n$  versus  $(Eu/Eu^*)_n$ . All low salinity fluorites associated with metalliferous mineralization plot with positive or negligible europium anomalies. These results agree well with those of Eppinger and Closs (1990).

$(\text{Ce}/\text{Ce}^*)_n$  vs  $(\text{Eu}/\text{Eu}^*)_n$ 

+ barren deposits

▽ Au/Ag, Eppinger and Closs (1990)

▼ Au/Ag, this study

⊠ high salinity base metals deposits

unreasonable to suggest that the conditions necessary to form positive europium anomalies exist solely in hydrothermal systems which contain base and/or precious metals. However, these conditions may be conducive to the precipitation of metals if they are present in the mineralizing solutions.

Europium, unlike the other REE, can exist as either a divalent or trivalent ion in aqueous solutions. The behavior of europium in hydrothermal solutions is controlled by  $\text{Eu}^{2+}/\text{Eu}^{3+}$  redox equilibria as well as fluid-mineral partitioning (Sverjensky, 1984). At temperatures near  $100^{\circ}\text{C}$ , fluids with  $f_{\text{O}_2}$  near the magnetite/hematite or sulfide/sulfate redox equilibria could contain significant concentrations of both  $\text{Eu}^{2+}$  and  $\text{Eu}^{3+}$ . Under these conditions, europium anomalies inherited from the source rocks can be preserved in the hydrothermal fluids. If the mineralizing fluids contain positive Eu anomalies they could transfer them to fluorite as long as oxygen fugacity is high enough to permit the oxidation of  $\text{Eu}^{2+}$  to  $\text{Eu}^{3+}$ . This is because  $\text{Eu}^{3+}$  substitutes for  $\text{Ca}^{2+}$  while  $\text{Eu}^{2+}$  is excluded from the fluorite structure because of its larger ionic radius. If the  $f_{\text{O}_2}$  is too low to allow for the conversion of  $\text{Eu}^{2+}$  to  $\text{Eu}^{3+}$ , any positive europium anomaly present in the fluid will not be reproduced in fluorite which precipitates from that fluid.

The presence of positive Eu anomalies may result from the destruction of feldspars which typically contain large

Eu anomalies. This would seem to suggest that more feldspar destruction has occurred in the low salinity base and/or precious metals fluorite systems than in the barren ones. However, the presence of cogenetic mineral phases such as barite could deplete solutions in Eu, and thereby preclude the development of positive Eu anomalies in coeval fluorite. Because of strong sulfate complexing of  $\text{Eu}^{2+}$ , barite almost invariably contains large positive Eu anomalies (Guichard et al., 1979). It is important to note that all "barren" fluorites with negligible or positive Eu anomalies are from deposits where barite is absent or is only a minor phase. However, negative Eu anomalies are also present in several deposits where barite is absent or minor.

At temperatures above about 250 °C,  $\text{Eu}^{3+}$  is unstable in aqueous solutions and is present nearly entirely as  $\text{Eu}^{2+}$ . Because  $\text{Eu}^{2+}$  does not substitute for  $\text{Ca}^{2+}$  in fluorite, high-temperature fluorites, such as those in the Capitan Mountains, contain large negative europium anomalies.

By itself, the range of Ce anomalies defined by the data of Eppinger and Closs (1990), and from this study, does not adequately differentiate fluorite associated with low temperature metalliferous deposits. Cerium may be present as either  $\text{Ce}^{3+}$  or as  $\text{Ce}^{4+}$ . Hydrothermal solutions may contain  $\text{Ce}^{3+}$  which, through coupled substitution, readily enters the fluorite structure. However,  $\text{Ce}^{4+}$  is immobile in hydrothermal solutions and is thus excluded from fluorite (Constantopoulos, 1988). Therefore, the presence of

negative Ce anomalies indicates that high oxygen fugacities were present and permitted the oxidation of  $Ce^{3+}$  to  $Ce^{4+}$ .

Three districts without known metalliferous mineralization, the Gila Fluorospar district, the Chise district, and Fluorite Ridge contain fluorite with positive or negligible europium anomalies. The Gila and Chise samples and three of the Fluorite Ridge samples also have Ce anomalies, Sc/Eu ratios and Sr contents which are similar to the low salinity metalliferous deposits. However, the Fluorite Ridge and Chise district samples have low (Tb/Yb)<sub>n</sub> ratios relative to the low salinity metalliferous deposits. One of the Gila Fluorospar district samples (FL36) has a (Tb/Yb)<sub>n</sub> ratio which is near that of the low salinity metalliferous deposits while the other (FL35) has a very large (Tb/Yb)<sub>n</sub> ratio.

#### SUMMARY AND CONCLUSIONS

Fluid inclusion and stable isotope data indicate that the bulk of the deposits formed from low salinity (< 8 eq. wt.% NaCl) variably-exchanged meteoric waters. A second set of deposits was formed from high salinity (9-20 eq. wt.% NaCl) fluids and includes those at Hansonburg, the Zuni Mountains, and the eastern slope of the Sierra Caballo. No signatures involving  $\delta D$ ,  $\delta^{18}O$ , Th, or salinity differentiate metalliferous deposits from barren ones. A weak correlation exists between  $\delta^{18}O$  and salinity further establishing the involvement of variably exchanged meteoric waters. No



correlations between isotopic or microthermometric data and trace and rare earth element data could be established.

Several factors could potentially affect fluorite composition and include: (1) the compositions of rocks which supplied trace and rare earth elements to the hydrothermal solutions, (2) the ability of those solutions to transport species under various geochemical conditions, (3) the presence of other mineral phases which preferentially incorporate certain elements, and (4) the ability of various elements to enter the fluorite structure under differing geochemical conditions. However, experimental data bearing on the controls of compositional variation in hydrothermal fluorite is quite limited. Although the specific controls on fluorite geochemistry are poorly understood, the results from this study are encouraging, as they suggest that fluorite geochemistry may reflect fluid conditions. However, the ability to model these fluid conditions would require much more experimental data than is currently available. This makes it necessary to approach fluorite geochemistry from a largely empirical standpoint. The geochemistry of fluorite deposits in southwestern New Mexico is influenced by host lithology as well as other controls which likely include temperature, salinity, fluid composition, pH, and  $f_{O_2}$ .

Although concentrations of most elements are similar among fluorites from a given district, their ranges show much overlap, making discrimination of deposit groups

difficult or impossible with many elements. However, concentrations of several elements including the REE, and Sc and Sr, consistently differentiate groups of deposits including low salinity base and/or precious metals deposits.

REE concentrations are generally predictable according to host lithology. This may allow for the detection of covered lithologic units which affected fluorite composition. Igneous rocks appear to have influenced fluorite compositions in sediment-hosted deposits in the Sierra Cuchillo and the southern Sierra Caballo.

Several variables including the Sc/Eu ratio, Sr concentration, (Tb/Yb)<sub>n</sub> ratio, and Eu anomalies constrain all fluorites associated with low salinity base and precious metals mineralization. It is important to note that these deposits occur in several districts and are hosted by a number of rock types including limestone, granodiorite, basalt, and andesite. The fact that these signatures exist is remarkable given that host-rock controls are so important to fluorite composition. Values of these variables in fluorite from the Gila fluorospar district are very similar to those of low salinity metalliferous deposits. For this reason, it appears that significant potential exists for the discovery of precious metals mineralization in the Gila Fluorospar district. No signatures were found which distinguish fluorite associated with high salinity base metals mineralization.

Interestingly, within the low salinity group of

deposits, REE and Sr contents tend to increase and Sc/Eu tends to decrease from east to west. Lamarre and Hodder (1978) propose a model to explain the spatial distribution of fluorite in the western United States which presumes subduction of oceanic crust during early to middle Tertiary time. This observed zonation may be consistent with such a model.

While the question of whether fluorite geochemistry may be useful as an exploration tool is still largely unanswered, it is apparent that fluorite composition varies in a somewhat predictable manner. In southwestern New Mexico, geochemical signatures successfully differentiate low salinity metalliferous deposits from barren ones. The geochemical signatures revealed in this study may or may not be applicable to mineral exploration outside of the study area. However, it has been shown that fluorite compositions are not random and that they do index host lithologies and deposit types. Therefore, one might expect that these or other signatures contained in fluorite may indicate low salinity base and/or precious metals mineralization in other regions. It would be of much interest to test the usefulness of fluorite geochemistry in precious metals exploration. Ultimately, this must be done by drilling in or near fluorite occurrences in a mining district which contains metalliferous deposits as well as apparently barren fluorite deposits.

## REFERENCES

- Akande, S. O. and Mucke, A., 1989, Mineralogical, textural, and paragenetic studies of the lead-zinc-copper mineralization in the lower Benue Trough (Nigeria) and their genetic implications, *J. African Earth Sciences*, v. 9, (1), pp. 23-29.
- Allen, M. S., and McLemore, V. T., 1991, The geology and petrogenesis of the Capitan pluton, New Mexico, *New Mexico Geol. Soc. Field Conf.*, 42nd Guidebook, pp. 115-127.
- Bigeleisen J., Perlman, M. L., and Prosser, H. C., 1952, Conversion of hydrogenic materials for isotopic analysis, *Anal. Chem.*, v. 24, pp. 1356-
- Bodnar, R. J., 1992, Revised equation and Table for freezing-point deperessions of H<sub>2</sub>O-salt fluid inclusions, *PACROFI IV, Program and Abstracts*, p 15.
- Chesley, J. T., Halliday, A. N., and Scrivener, R. C., 1991, Samarium-neodymium direct dating of fluorite mineralization, *Science*, v. 252, pp. 949-951.
- Constantopoulos, J., 1988, Fluid inclusions and rare earth element geochemistry of fluorite from South-Central Idaho, *Econ. Geol.*, v. 83, pp. 626-636.
- Criss, R. E., and Taylor, H. P. Jr., 1986, Meteoric-hydrothermal systems, *in* Stable isotopes in high temperature geological processes, Valley, J. W., Taylor, H. P., and O'Neil, J. R. (eds.), *Reviews in Mineralogy*, v. 16, pp. 373-422.
- Dunham, D. C., 1935, The geology of the Organ Mountains, *New Mexico Bur. of Mines and Min. Resources, Bull.* 11, 272 p.
- Ekambaram, V., Brookins, D. G., Rosenberg, P. E., and Emanuel, K. M., 1986, Rare earth element geochemistry of fluorite-carbonate deposits in Western Montana, USA, *Chem. Geol.* v. 54, pp. 319-331.
- Elston, W. E., Erb, E. E., and Deal, E. G., 1979, Tertiary geology of Hidalgo County, New Mexico; guide to metals, industrial minerals, petroleum, and geothermal resources, *N. M. Geol.*, v. 1, (1), pp. 1-6.
- Elston, W. E., 1961, Upper Cretaceous volcanism and mineralization in Steeple Rock mining district, Grant County, New Mexico, *NM Geol. Soc.*, Guidebook, 12th field conference, p. 193.
- Eppinger, R. G., 1988, Trace and rare earth element variation in fluorites collected from skarn and epithermal mineral deposits in the Sierra Cuchillo area, south-central New Mexico, *USGS Open File Rept.*, OF 88-0566, 108p.
- Eppinger, R. G., and Closs, L. G., 1990, Variation of trace elements and rare earth elements in fluorite: a possible tool for exploration, *Econ. Geol.*, v. 85, pp. 1896-1907.
- Fleischer, M., 1969, The lanthanide elements in fluorite, *The Indian Mineralogist*, v. 10, pp. 36-39.
- Friedman, I., and O'Neil, J. R., 1977, Compilation of stable isotope fractionation factors of geochemical interest, *in* Fleischer, M., (ed.) *Data of geochemistry*, Sixth edition, *USGS Prof. Pap.* 440-KK, pp. KK1-KK12.
- Galindo, C., Tornos, F., Darbyshire, D. P. F., and Casquet, C., 1994, The age and origin of the barite-fluorite (Pb-Zn) veins of the Sierra del Guadarrama (Spanish Central

- System, Spain); a radiogenic (Nd, Sr) and stable isotope study, *Chem. Geol.*, v. 112, (3-4), pp. 351-364.
- Ganzeyev, A. A., and Sotskov, Y. P., 1976, Rare earth elements in fluorites of different origin, *Geochem. Internat.*, v. 3, pp. 51-56.
- Gilder, S. A., 1989, *Geochemistry of fluorite in the caldera environment*, Unpub. M. S. thesis, Univ. of Texas-El Paso, 167 p.
- Gillerman, E., 1952, Fluorospar deposits of Burro Mountains and vicinity, Grant County, New Mexico, *USGS -Bulletin*, B 0973-F, pp. 261-289.
- Gillerman, E., 1964, Mineral deposits of western Grant County, New Mexico, *New Mexico Bur. Mines and Min. Res.*, Bull. 83, 213 p.
- Griswold, G. B., 1961, Mineral Deposits of Luna County, New Mexico, *NM Bur. Mines and Min. Res. Bull.* 72, 157p.
- Guichard, F., Church, T. M., Treuil, M., and Jaffrezic, H., 1979, Rare earths in barites: distribution and effects on aqueous partitioning, *Geochim. Cosmochim. Acta*, v. 43, pp. 983-997.
- Halliday, A. N., Shepherd, T. J., Dickin, A. P., and Chesley, J. T., 1990, Sm-Nd evidence for the age and origin of a Mississippi Valley type ore deposit, *Nature*, v. 344, pp. 54-56.
- Harley, G. T., 1934, The geology and ore deposits of Sierra County, New Mexico, *New Mexico Bur. of Mines and Min. Resources*, Bull. 10, 219 p.
- Harrison, R. W., 1986, General geology of the Chloride mining district, Sierra and Catron Counties, New Mexico, *Geol. Soc. Field Conf.*, 37th, Guidebook, pp. 265-272.
- Hewitt, C. H., 1959, Geology and mineral deposits of the northern Big Burro Mountains-Redrock area, Grant County, New Mexico, *NM Bur. Mines and Min. Res. Bull.* 60, 151p.
- Huskinson, E. J., 1974, Geology and fluorospar deposits of the Chise fluorospar district, Sierra County, New Mexico, Unpub. M. S. thesis, Univ. Texas-El Paso, 74p.
- Jahns, R. H., McMillan, D. K., O'Brient, J. D., and Fisher, D. L., 1978, Geologic section in the Sierra Cuchillo and flanking areas, Sierra and Socorro Counties, New Mexico, *Geol. Soc. New Mexico Spec. Pub.* 7, pp 131-138.
- Kelley, V. C., 1971, Geology of the Pecos country, southeastern New Mexico, *New Mexico Bur. Mines and Mineral Res.*, Memoir 24, 75 p.
- Kessler, S. E., 1977, Geochemistry of manto fluorite deposits, northern Coahuila, Mexico, *Econ. Geol.*, v. 72, (2), pp. 204-218.
- Kishima, N., and Sakai, H., 1980, Oxygen-18 and deuterium determination on a single water sample of a few milligrams, *Anal. Chem.*, v. 52, pp. 356-358.
- Kottowski, F. E., and Steensma, R. S., 1979, Barite-fluorite-lead mines of Hansonburg mining district in central New Mexico, *New Mexico Geology*, v. 1, n.2, pp. 17-32.
- Lamarre, A. L., and Hodder, R. W., 1978, Distribution and genesis of fluorite deposits in the Western United States and their significance to metallogeny, *Geology*, v. 6, pp. 236-238.
- Lasky, S. G., 1938, Geology and ore deposits of the Lordburg mining district, Hidalgo County, New Mexico, *USGS Bull.* B 0885, 62 p.

- Lindstrom, D. J., and Korotev, R. L., 1982, TEABAGS: Computer program for instrumental neutron activation analysis, *Jour. Radioanalytical Chem.*, v. 40, pp. 93-114.
- McLemore, V. T., 1980, Geology of the Precambrian rocks of the Lemitar Mountains, Socorro County, New Mexico, Unpub. M. S. thesis, New Mexico Inst. of Mining and Tech., 169p.
- McLemore, V. T., 1994, Geology and geochemistry of the mineralization and alteration in the Steeple Rock district, Grant County, New Mexico and Greenlee County, Arizona, Unpub. PhD dissertation, Univ. Texas at El Paso, 525 p.
- McAnulty, W. N., 1978, Fluorospars in New Mexico, New Mexico Bureau of Mines and Mineral Resources Memoir 34.
- McOwen, L. K., 1993, The Brock Canyon volcanic complex, Grant County, New Mexico: Volcanic evolution, alteration, and mineralization, Unpub. M. S. thesis, Univ. of Arizona, 167 p.
- Moller, P. Parekh, P. P., and Schneider, H. J., 1976, The application of Tb/Ca-Tb/La abundance ratios to problems of fluorospars genesis, *Min. Deposita*, v. 11, pp. 111-116.
- Moller, P., and Morteani, G., 1983, On the geochemical fractionation of rare earth elements during the formation of Ca minerals and its application to problems of the genesis of ore deposits, *in* Augustithis, S. S. (ed.), *The significance of trace elements in solving petrogenetic problems and controversies*, Athens, Theophrastus Pub., pp. 747-791.
- Morse, A. D., Wright, I. P., and Pillinger, C. T., 1993, An investigation into the cause of memory effects associated with the conversion of H<sub>2</sub>O to H<sub>2</sub> for D/H measurement, *Chem. Geol.*, v. 107, (1-2), pp. 147-158.
- Nakamura, N., 1974, Determination of REE, Ba, Fe, Mg, Na, and K in carbonaceous and ordinary chondrites, *Geochim. et Cosmochim. Acta*, v. 38, pp. 757-775.
- North, R. M., and McLemore, V. T., 1985, Geology and mineralization of the El Cuervo Butte barite-fluorite-galena deposit in Southern Santa Fe County, New Mexico, *New Mexico Geol. Soc. Guidebook*, 36th Field Conference, Santa Rosa, pp. 301-305.
- North, R. M., and Tuff, M. A., 1986, Fluid-inclusion and trace-element analyses of some barite-fluorite deposits in South-Central New Mexico, *New Mexico Geol. Soc. Guidebook*, 37th Field Conference, Truth or Consequences, pp. 301-306.
- Peters, W. C., 1958, Geologic characteristics of fluorospars deposits in the western United States, *Econ. Geol.*, v. 53, (6), pp. 663-688.
- Phillips, R. S., 1990, Geochemistry of hydrothermal Th-U-REE quartz/fluorite veins from the Capitan pluton, Unpub. M. S. thesis, New Mexico Inst. of Mining and Tech., 202 p.
- Phillips, R. S., Campbell, A. R., and McLemore, V. T., 1991, Th-U-REE quartz/fluorite veins, Capitan pluton, New Mexico: evidence for a magmatic/hydrothermal origin, *New Mexico Geol. Soc. Field Conf.*, 42nd Guidebook, pp. 129-136.
- Putnam, Borden III, 1980, Fluid inclusion and microchemical analysis of the Hansonburg Mississippi Valley-Type ore deposits in Central New Mexico, Unpub. M. S. thesis, New Mexico Inst. of Mining and Tech., 156 p.

- Ratte', J.C., Gaskill, D. L., Eaton, G. P., Peterson, D. L., Stotelmeyer, R. B., and Meeves, H. C., 1979, Mineral resources of the Gila Primitive Area and Gila Wilderness, New Mexico, USGS Bull. 1451, 229 p.
- Richardson, C. K. and Holland, H. D., 1979, The solubility of fluorite in hydrothermal solutions; an experimental study, *Geochim. Cosmochim. Acta*, v. 43, (8), pp. 1313-1326.
- Roedder, E., 1984, Fluid inclusions, *in* Ribbe, P. H. (ed.), *Reviews in Mineralogy*, v. 12, 646 p.
- Rothrock, H. E., Johnson, C. H., and Hahn, A. D., 1946, Fluorospar resources of New Mexico, New Mexico Bureau of Mines and Mineral Resources, Bull. 21, 245 p.
- Ruff, R., 1994, Gas analysis of fluid inclusions: Application toward precious metals exploration, Steeple Rock mining district, Grant County, New Mexico, Unpub. M. S. thesis, New Mexico Inst. of Mining and Technology, 93 p.
- Ruiz, J., Kesler, S. E., Jones, L. M., and Sutter, J. F., 1980, Geology and geochemistry of the Las Cuevas fluorite deposit, San Luis Potosi, Mexico, *Econ. Geol.*, v. 75, pp. 1200-1209.
- Ruiz, J., Kesler, S. E., and Jones, L. M., 1985, Strontium isotope geochemistry of fluorite mineralization associated with fluorine-rich igneous rocks from the Sierra Madre Occidental, Mexico: Possible exploration significance, *Econ. Geol.*, v. 80, pp. 33-42.
- Schneider, H. J., Moller, P., Parakh, P. P., 1975, Rare earth element distribution in fluorites and carbonate sediments of the East-Alpine Mid-Triassic sequences in the Nordliche Kalkalpen, *Min. Deposita.*, v. 10, pp. 330-344.
- Strong, D. F., Fryer, B. J., and Kerrich, R., 1984, Genesis of the St. Lawrence fluorospar deposits as indicated by fluid inclusion, rare earth element, and isotopic data, *Econ. Geol.*, v. 78, pp. 1142-1158.
- Sverjenski, D. A., 1984, Europium redox equilibria in aqueous solution, *Earth and Plan. Sci. Let.*, v. 67, pp. 70-78.
- Taggart, J. E. Jr., Rosenzweig, A., and Foord, E. E., 1989, The Hansonburg district, Bingham, New Mexico, *The Mineralogical Record*, v. 20, pp. 31-46.
- Woodward, T. M., 1973, Geology of the Lemitar Mountains, Socorro County, New Mexico, Unpub. M. S. thesis, New Mexico Inst. of Mining and Tech., 73 p.

Appendix I. Fluid inclusion microthermometry  
 p - primary, ps - pseudosecondary, s - secondary  
 salinity (wt.% cNaCl), Th (C)

sample number	type	inclusion number	inclusion number									
			1	2	3	4	5	6	7	8	9	
FL1	p	salinity	1.4	1.3	1.74		1.3	1.3	1.57	1.9	2.07	1.9
	Th	salinity	309	255	301	251	296	228	322	405	258	
	s	salinity	0.88	0.88								
	Th	salinity	136	130								
FL5	p	salinity	0.88	1.05	0.88	0.88	1.23	1.05	0.88	1.23	1.23	1.23
	Th	salinity	183	187	185	180	177	199	200	183	198	
	ps	salinity	1.23	1.23	1.4	1.05						
	Th	salinity	192	193	174	197						
	s	salinity	1.23	1.23	1.23	1.23	1.4	1.57	1.4	1.4	1.4	
	Th	salinity	191	191	206	200	196	201	199	194	194	
FL7	p	salinity	4.65	4.65	4.8	4.96	5.41	4.96	4.96	3.39	3.39	5.11
	Th	salinity	181	181	185	183	184	185	184	184	189	184
	ps	salinity	8.14	8.14	8.14	1.4	3.39	1.4	1.4	1.4	1.4	
	Th	salinity	171	171	171	139	144	150	161	154		
	s	salinity	1.4	1.23	1.4	1.4	0.88	0.88	1.74	1.23	2.07	
	Th	salinity	134	133	135	139	122	124	141	143	147	
FL8	p	salinity	6.01	6.3	6.59	6.16	5.71	5.71	5.86	6.01	6.16	6.16
	Th	salinity	172	177	181	185	183	183	183	183	183	184
	s	salinity	4.49	4.34	4.49	3.39	3.39					
	Th	salinity	170	171	152	171	170					
FL9	p	salinity	6.3	4.34	4.34							
	Th	salinity	203	212	218							
	ps	salinity	4.8	4.8	4.8	4.8						
	Th	salinity	170	176	191	198						



Appendix I (continued). Fluid inclusion microthermometry  
 p - primary, ps - pseudosecondary, s - secondary  
 salinity (wt.% eNaCl), Th (C)

sample number	type	inclusion number	11	12	13	14	15	16	17	18	19
FL1	p	salinity	1.9	2.07							
		Th	238	249							
	s	salinity									
		Th									
FL5	p	salinity	1.23	1.23	1.91	1.4	1.05	1.57			
		Th	192	193	193	184	197	188			
	ps	salinity									
		Th									
	s	salinity									
		Th									
FL7	p	salinity									
		Th									
	ps	salinity									
		Th									
	s	salinity	1.74								
		Th	126								
FL8	p	salinity	6.45	5.26	5.56	5.71	5.71	5.71	5.71	6.01	6.16
		Th	184	181	178	178	181	182	178	183	182
	s	salinity									
		Th									
FL9	p	salinity									
		Th									
	ps	salinity									
		Th									





Appendix I (continued). Fluid inclusion microthermometry  
 p - primary, ps - pseudosecondary, s - secondary  
 salinity (wt.% eNaCl), Th (C)

FL18	p	salinity	1.91	1.91	2.74	2.07	2.57	1.05	1.05	1.05	1.05	1.05	1.05	1.05	1.05	1.05	1.05	1.05	1.05
		Th	174	174	170	169	170	171	169	170	171	169	170	171	169	170	171	169	170
	s	salinity	1.4	1.91	1.91														
		Th	173	173	171														
FL19	p	salinity	5.56	5.56	5.56	5.56	5.41	5.56	5.56	5.56	5.56	5.56	5.56	5.56	5.56	5.56	5.56	5.56	5.56
		Th	176	178	180	194	200	181	196	181	196	181	196	181	196	181	196	181	196
	ps	salinity	8.41	8.41	5.56	5.56													
		Th	189	189	201	203													
FL20	p	salinity	1.91	1.91	1.91	1.74	1.91	1.91	1.91	1.91	1.91	1.91	1.91	1.91	1.91	1.91	1.91	1.91	1.91
		Th	150	158	152	164	161	162	159	162	159	162	159	162	159	162	159	162	159
	s	salinity	1.91	1.91	1.74	1.91	1.91												
		Th	187	186	159	158	182												
FL24	p	salinity	2.07	2.07	2.07	2.07	2.07	2.41	2.41	2.41	2.41	2.41	2.41	2.41	2.41	2.41	2.41	2.41	2.41
		Th	161	150	184	171	158	178	188	178	188	178	188	178	188	178	188	178	188
	s	salinity	2.07	3.06	3.06														
		Th	183	192	163														
FL25	p	salinity	1.4	0.88	0.88	0.88	0.88	0.88	0.88	0.88	0.88	0.88	0.88	0.88	0.88	0.88	0.88	0.88	0.88
		Th	180	197	198	173	172	206	180	206	180	206	180	206	180	206	180	206	180
	s	salinity	0.53	0.53															
		Th	156	156															
FL26	p	salinity	7.73	7.73	7.73	8	8.14	7.45	7.45	7.45	7.45	7.45	7.45	7.45	7.45	7.45	7.45	7.45	7.45
		Th	220	222	218	230	223	217	218	221	218	221	218	221	218	221	218	221	218
	s	salinity	4.03	4.03															
		Th	173	170															
FL27	p	salinity	0.88	1.23	1.23	1.23	1.23	1.23	1.23	1.23	1.23	1.23	1.23	1.23	1.23	1.23	1.23	1.23	1.23
		Th	182	186	181	184	168	169	168	171	168	171	168	171	168	171	168	171	168



Appendix I (continued). Fluid inclusion microthermometry  
 p - primary, ps - pseudosecondary, s - secondary  
 salinity ( wt.% eNaCl), Th (C)

FL29	p	salinity	2.07	2.41	0.53	0.53	9.47	8.81	4.49				
	Th		170	167	169	167	202	194	169				
FL30	p	salinity	0.53	0.53	1.91	0.71	0.71	1.4	1.4	0.53			
	Th		142	169	169	166	172	159	167	166			
	s	salinity	0.53	0.53	0.53								
	Th		177	171	155								
FL31	p	salinity	0.71	0.71	0.53	0.88	0.88	0.53	0.35	0.53	0.53	0.53	0.53
	Th		171	168	169	177	173	173	167	169	169	173	173
	s	salinity	1.23										
	Th		140										
FL32	p	salinity	1.23	1.23	1.05	1.23	1.23	0.88	0.88	0.88	0.88	0.88	0.88
	Th		143	132	133	138	137	130	132	146	146	146	0.88
FL33	p	salinity	1.05	1.05	1.23	0.88	1.05	0.88	0.88	0.88	0.88	0.88	0.88
	Th		165	152	166	159	160	164	160	160	160	160	156
	s	salinity	0.88	0.88	0.88								
	Th		190	151	152								
FL34	p	salinity	1.74	1.74	1.57	1.57	1.05	1.05	1.4	1.4	1.4	1.4	1.57
	Th		169	175	165	162	160	167	170	171	171	162	162
	ps	salinity	1.74	1.74	1.74	1.57	1.57	1.57	0.88	0.88	0.88	0.88	0.88
	Th		164	164	165	167	165	162	168	167	167	167	167
FL35	p	salinity	3.06	2.24	1.74	2.24	1.91	2.57	2.74	3.23	3.23	3.39	3.39
	Th		193	195	179	172	160	164	167	172	172	170	170
	ps	salinity	5.11	5.11									
	Th		176	174									
	s	salinity	4.96	2.74	2.74								
	Th		170	167	161								



Appendix I (continued): Fluid inclusion microthermometry  
 p - primary, ps - pseudosecondary, s - secondary  
 salinity ( wt.% eNaCl), Th (C)

FL36	p	salinity	1.05	0.71	0.88	0.71	0.71													
		Th	220	222	223	242	187													
FL37	p	salinity	2.07	1.74	1.91	1.4	1.23	0.88	0.88	1.23										
		Th	214	215	215	189	187	154	152	199										
	s	salinity	1.23	1.23	1.05															
		Th	173	176	179															
FL50	p	salinity	12.96	12.85	14.97	15.07	15.07	14.97	19.37	20.37										
		Th	139	149	139	140	140	143	153	141										
FL51	p	salinity	7.59	7.45	9.34	7.17	7.17	7.31	7.31	8.41										
		Th	204	210	108	220	220	147	125	127										
	ps	salinity	8.41	7.73	7.59	8.55	13.29	13.4	7.31	7.45										
		Th	135	130	139	159	146	135	176	157										



Appendix I (continued). Fluid inclusion microthermometry  
 p - primary, ps - pseudosecondary, s - secondary  
 salinity (wt.% cNaCl), Th (C)

FL36	p	salinity																		
		Th																		
FL37	p	salinity	1.05	1.05	0.88	0.88	1.05	1.05	1.05	1.05	1.05	1.05	1.05	1.05	1.05	1.05	1.05	1.05	1.05	1.05
		Th	195	192	194	195	194	194	194	191	191	191	191	191	191	191	191	191	191	191
	s	salinity																		
		Th																		
FL50	p	salinity	20.22	20.45	20.22	12.28	12.39	18.04	11.34											
		Th	142	139	142	140	140	140	136											
FL51	p	salinity																		
		Th																		
	ps	salinity																		
		Th																		

Appendix II.  
 $\delta D$  and  $\delta^{18}O$  data.  
 (see appendix IV for explanation of methods)

sample number	lab number	$\delta^{18}O_{H_2O}$ (SMOW)	$\delta D_s$ (SMOW)	$\delta D_s+4$	$\mu\text{molCO}_2$ added	$\mu\text{molCO}_2$ recovered	mg $H_2O$
FL12	HU/CO <sub>2</sub> 34-5	-5.2	-59	-55	19	19	1.4
FL31	HU/CO <sub>2</sub> 36-1	-3.9	-38	-34	19	19	3.6
FL30	HU/CO <sub>2</sub> 36-2	4.1	-33	-29	18	19	9.7
FL32	HU/CO <sub>2</sub> 36-3	-1.2	-79	-75	19	23	5.9
FL34	HU/CO <sub>2</sub> 36-4	1.7	-62	-58	18	24	4.4
FL16	HU/CO <sub>2</sub> 38-2	1.3	-66	-62	19	19	1.7
FL17	HU/CO <sub>2</sub> 38-3	-2.5	-56	-52	19	19	7.7
FL18	HU/CO <sub>2</sub> 38-4	-1.6	-56	-52	19	19	4.5
FL19	HU/CO <sub>2</sub> 38-5	2.1	-54	-50	19	19	17.0
FL1	HU/CO <sub>2</sub> 40-1	-8.6	-87	-83	19	23	2.8
FL5	HU/CO <sub>2</sub> 40-2	-7.2	-66	-62	19	19	3.6
FL7	HU/CO <sub>2</sub> 40-3	2.1	-31	-27	19	19	1.4
FL9	HU/CO <sub>2</sub> 40-5	-8.3	-75	-71	19	20	9.5
FL24	HU/CO <sub>2</sub> 40-6	-6.7	-61	-57	19	18	13.3
FL10	HU/CO <sub>2</sub> 44-1	-6.0	-57	-53	18	21	10.5
FL14	HU/CO <sub>2</sub> 44-3	0.7	-62	-58	17	18	17.0
FL15	HU/CO <sub>2</sub> 44-4	1.6	-60	-56	18	17	7.8
FL20	HU/CO <sub>2</sub> 44-5	-8.4	-75	-71	19	19	7.0
FL26	HU/CO <sub>2</sub> 46-1	5.5	-55	-51	19	20	9.5
FL25	HU/CO <sub>2</sub> 46-2	-6	-71	-67	18	18	7.3
FL40	HU/CO <sub>2</sub> 46-5	-1.5	-66	-62	19	19	0.9
FL42	HU/CO <sub>2</sub> 46-6	0.2	-43	-39	19	19	13.8
CPU-1	HU/CO <sub>2</sub> 47-2	2.0	-87	-83	20	20	0.7

Appendix II (continued).  
 $\delta D$  and  $\delta^{18}O$  data.  
 (see appendix IV for explanation of methods)

sample number	lab number	$\delta^{18}O_{H_2O}$ (SMOW)	$\delta D_s$ (SMOW)	$\delta D_{s+4}$	$\mu\text{molCO}_2$ added	$\mu\text{molCO}_2$ recovered	mg $H_2O$
FL50	HU/CO <sub>2</sub> 47-3	-4.9	-85	-81	20	20	2.0
FL51	HU/CO <sub>2</sub> 47-4	-1.1	-94	-90	19	18	1.6
FL36	HU/CO <sub>2</sub> 47-6	-1.6	-61	-57	18	18	1.8
FL37	HU/CO <sub>2</sub> 48-1	-3.3	-91	-87	20	20	0.9
FL35	HU/CO <sub>2</sub> 48-2	-1.7	-61	-57	19	19	17.0
FL43	HU/CO <sub>2</sub> 48-4	-9.9	-112	-108	20	20	3.7
FL28	HU/CO <sub>2</sub> 48-5	-1.9	-65	-61	20	17	13.8
FL43	HU/CO <sub>2</sub> 50-1	-14.6	-102	-98	19	20	2.1
FL8	HU/CO <sub>2</sub> 50-3	-2.4	-63	-59	18	20	3.8
FL29	HU/CO <sub>2</sub> 50-4	-2.4	-63	-59	19	21	2.1
W3-4	HU/CO <sub>2</sub> 50-6	-0.1	-90	-86	19	19	1.3

## Appendix III.

Trace and rare earth element data from INAA and XRF.

n.d. - abundance not determined.

sample number	element (ppm)								
	La	Ce	Nd	Sm	Eu	Tb	Yb	Lu	REE sum
FL1	33.4	42.0	34	11.6	2.99	3.30	13.92	1.79	143.0
FL5	17.9	23.3	9	2.1	0.67	0.35	0.97	0.12	54.7
FL7	1.9	3.2	2	0.4	0.05	0.07	0.19	0.02	7.4
FL8	3.8	9.4	5	1.5	0.26	0.40	1.37	0.16	21.4
FL9	2.2	4.7	2	0.8	0.20	0.41	1.77	0.20	12.5
FL10	1.5	2.0	n.d.	0.4	0.10	0.09	0.28	0.04	4.3
FL12	16.6	36.1	14	4.2	1.35	1.05	4.86	0.68	78.7
FL13	0.6	1.3	1	0.2	0.05	0.05	0.13	0.02	3.3
FL14	1.1	1.8	1	0.3	0.04	0.05	0.04	n.d.	4.5
FL15	0.4	0.8	n.d.	0.1	0.02	0.03	0.03	n.d.	1.4
FL16	15.7	16.7	8	1.5	0.39	0.34	1.65	0.24	44.8
FL17	9.7	20.8	9	2.3	0.50	0.56	1.33	0.16	44.1
FL18	1.0	2.5	2	0.9	0.30	0.31	0.65	0.08	7.7
FL19	2.6	4.7	4	1.7	0.43	0.33	0.53	0.06	14.8
FL20	3.9	5.5	3	0.7	0.20	0.09	0.13	0.02	13.8
FL24	7.2	16.2	10	3.1	1.29	0.90	2.03	0.23	40.7
FL25	3.6	8.1	5	1.0	0.31	0.24	0.61	0.07	18.5
FL26	6.3	13.1	6	1.8	0.68	0.39	0.80	0.09	29.6
FL27	9.6	9.3	9	2.2	0.77	0.58	1.94	0.24	33.3
FL28	5.6	7.0	8	2.4	0.90	0.98	3.52	0.45	28.3
FL29	18.1	42.3	23	9.0	2.58	2.46	3.40	0.38	100.8
FL30	23.3	43.4	23	5.1	1.81	0.68	0.95	0.11	98.5
FL31	22.9	46.6	27	10.2	5.80	2.42	3.61	0.45	118.8
FL32	12.6	27.4	16	6.1	2.23	2.21	10.86	1.59	79.3
FL33	5.7	11.9	7	3.7	1.33	1.10	3.76	0.48	34.7
FL34	4.0	11.0	7	5.1	2.07	3.12	15.72	1.94	49.7
FL35	18.8	35.5	13	1.5	0.71	0.08	0.03	0.01	69.1
FL36	17.8	28.3	11	3.3	1.83	0.89	1.50	0.17	65.1
FL37	6.2	13.5	7	1.7	0.68	0.40	0.58	0.06	29.8
FL39	1.7	4.6	4	2.3	0.96	1.15	1.28	0.12	15.9
FL40	1.3	2.9	2	0.7	0.24	0.29	0.47	0.05	8.2
FL41	0.9	1.5	1	0.3	0.12	0.17	0.29	0.03	4.3
FL42	6.0	10.7	3	0.9	0.17	0.17	0.44	0.06	21.8
FL43	1.5	3.1	2	0.4	0.11	0.15	0.37	0.04	7.6
FL50	12.3	32.7	30	19.7	3.52	7.92	24.16	3.05	133.2
FL51	16.0	38.7	40	22.6	5.61	7.05	31.00	3.84	165.2
CPU-1	9.2	25.5	17	6.7	0.50	2.41	18.39	2.60	81.8
McCory	14.7	40.0	30	13.3	1.10	4.37	22.93	3.00	128.9
FN	16.4	48.3	36	14.8	0.89	4.48	27.04	3.81	151.6
CM239	17.2	43.7	24	6.7	0.65	1.88	14.20	2.11	110.3
KS-1	11.4	35.5	28	11.4	1.05	3.79	22.67	3.32	117.4
W3-4	14.3	40.4	35	12.5	0.83	3.59	20.87	3.04	130.5
W3-6	19.5	54.2	37	11.3	0.77	2.90	16.29	2.43	144.6

## Appendix III (continued).

Trace and rare earth element data from INAA and XRF.

n.d. - abundance not determined.

sample number	element (ppm)								
	Cs	Na	U	Sc	Fe	Zn	Th	Cu	Ni
FL1	0.1	0	0.3	0.4	107	3	0.5	10	20
FL5	0.0	12	0.1	0.0	29	1	0.0	15	11
FL7	0.0	6	0.0	0.0	78	2	0.1	13	3
FL8	0.0	11	0.2	0.0	19	4	0.1	12	11
FL9	n.d.	11	n.d.	0.1	13	13	0.1	19	9
FL10	0.1	33	0.1	0.1	28	1	0.1	29	7
FL12	0.0	29	0.2	0.3	23	n.d.	0.2	16	11
FL13	0.1	37	0.0	0.1	68	3	0.2	28	8
FL14	0.0	34	0.1	0.0	n.d.	1	0.0	19	3
FL15	0.1	32	0.1	0.1	n.d.	1	0.1	n.d.	5
FL16	n.d.	11	0.2	1.1	n.d.	1	0.1	12	6
FL17	n.d.	10	0.1	0.1	n.d.	1	0.1	13	9
FL18	n.d.	4	0.1	0.3	8	1	0.4	12	7
FL19	0.0	17	0.0	0.0	n.d.	0	0.1	11	1
FL20	0.0	9	n.d.	0.0	24	1	0.0	n.d.	5
FL24	0.1	10	n.d.	0.2	n.d.	1	0.0	14	14
FL25	0.1	16	n.d.	0.1	35	1	0.1	11	13
FL26	0.1	16	n.d.	0.0	19	1	0.1	16	8
FL27	0.1	18	n.d.	0.1	49	2	0.1	16	9
FL28	0.1	11	0.1	0.4	n.d.	1	0.1	10	14
FL29	0.0	22	0.2	0.0	16	1	n.d.	12	8
FL30	0.1	15	n.d.	0.1	37	1	0.2	12	9
FL31	0.1	0	n.d.	0.0	n.d.	7	0.1	14	11
FL32	n.d.	21	0.2	0.9	n.d.	2	0.5	11	13
FL33	0.0	12	0.1	0.1	16	3	n.d.	12	10
FL34	n.d.	24	0.5	0.7	25	1	0.1	13	19
FL35	0.0	6	n.d.	0.0	13	n.d.	n.d.	20	8
FL36	n.d.	9	0.1	0.0	16	1	n.d.	63	40
FL37	0.1	13	n.d.	0.0	n.d.	1	0.0	12	10
FL39	n.d.	30	0.1	0.3	n.d.	4	0.2	17	11
FL40	n.d.	13	n.d.	0.1	n.d.	1	0.1	18	9
FL41	0.0	10	n.d.	0.0	10	1	0.0	12	10
FL42	n.d.	10	0.1	0.0	n.d.	1	n.d.	13	5
FL43	0.2	7	n.d.	0.4	91	11	0.5	24	8
FL50	n.d.	77	n.d.	0.0	33	n.d.	1.8	41	51
FL51	0.1	90	n.d.	0.2	291	3	0.6	25	55
CPU-1	0.0	7	0.3	0.0	n.d.	1	n.d.	14	41
McCory	n.d.	10	0.4	0.0	n.d.	2	0.1		
FN	n.d.	93	0.4	0.0	180	n.d.	0.1		
CM239	n.d.	69	0.3	0.0	n.d.	n.d.	0.1		
KS-1	n.d.	65	n.d.	0.0	n.d.	n.d.	0.4		
W3-4	n.d.	85	0.2	0.0	n.d.	n.d.	0.1		
W3-6	n.d.	100	0.3	0.0	15	2	0.1		

## Appendix III (continued).

Trace and rare earth element data from INAA and XRF.  
n.d. - abundance not determined.

sample number	element (ppm)				
	Pb	Rb	Sr (XRF)	Sr (INAA)	Y
FL1	15	6	112	120	n.d.
FL5	14	4	77	77	26
FL7	44	4	30	37	17
FL8	86	n.d.	160	185	125
FL9	17	3	49	61	126
FL10	15	4	105	112	23
FL12	15	4	158	165	82
FL13	14	3	19	n.d.	13
FL14	10	n.d.	19	14.9	12
FL15	16	n.d.	20	19	8
FL16	13	3	39	42	40
FL17	14	3	59	70	35
FL18	21	5	113	124	44
FL19	8	n.d.	230	231	26
FL20	17	4	70	79	10
FL24	15	4	47	49	103
FL25	14	3	41	35	33
FL26	17	10	60	63	36
FL27	33	4	42	34	68
FL28	28	5	39	53	122
FL29	24	3	99	101	138
FL30	18	3	98	96	32
FL31	17	5	110	116	114
FL32	14	3	58	62	234
FL33	14	n.d.	48	51	51
FL34	15	n.d.	113	117	265
FL35	16	4	85	90	3
FL36	10	3	62	59	60
FL37	7	3	75	81	52
FL39	740	n.d.	168	161	146
FL40	14	4	22	26	67
FL41	57	4	19	12	51
FL42	14	n.d.	72	64	12
FL43	13	5	13	n.d.	38
FL50	21	4	24	n.d.	967
FL51	15	4	38	68	1147
CPU-1	14	n.d.	129	130	744
McCorv				126	
FN				149	
CM239				135	
KS-1				127	
W3-4				130	
W3-6				136	

## Appendix IV.

### H<sub>2</sub>O/CO<sub>2</sub> Microequilibration and Uranium reduction procedures

#### *H<sub>2</sub>O/CO<sub>2</sub> microequilibration*

The H<sub>2</sub>O/CO<sub>2</sub> microequilibration technique of (Kishima and Sakai, 1980) was modified for use in the Stable Isotope Laboratory at New Mexico Institute of Mining and Technology. Microequilibration vessels with 0.5 cm<sup>3</sup> volumes were utilized in order to ensure that small water volumes (1-15 μl) would exist mainly in the liquid rather than a vapor state. Maintaining water in a liquid state is important because oxygen exchange occurs most readily between liquid water and CO<sub>2</sub> vapor. The exchange reaction is probably facilitated by the formation of H<sub>2</sub>CO<sub>3</sub> (Arehardt, 1993, pers. comm.). Because <sup>18</sup>O is strongly fractionated between the liquid and vapor phases of water (Friedman and O'Neil, 1977), the portion present as a vapor must be minimized.

#### *Procedure*

Fluorite was crushed and sieved to -10/+40 mesh, hand picked for impurities, and cleaned in NaOH and then in HCl. After thorough oven drying, approximately 10-18g aliquots were loaded into quartz tubes, placed onto a vacuum line, and evacuated for 20-30 minutes. The samples were then heated to 800 C in a convection furnace for 10-15 minutes. Inclusion fluids were transferred through a small volume of

vacuum line and collected in microequilibration vessels via cryogenic pumping.

After collection of the inclusion fluids, the water portions were frozen in the equilibration vessels using an ethylene glycol/CO<sub>2</sub> slush and non-condensed gasses were removed. Approximately 20  $\mu$ moles of pure CO<sub>2</sub> of known isotopic composition was measured and added to each vessel. Pressures within the equilibration vessels were calculated to be about 2 atmospheres. H<sub>2</sub>O/CO<sub>2</sub> microequilibrations were carried out in a water bath at 44-45 °C for at least 72 hours. This time period was determined to exceed the minimum time needed for complete equilibration. At the completion of equilibration the vessels were placed on-line and the water was refrozen in situ. The yield of condensable gas was measured and bottled for analysis. The water was then converted to H<sub>2</sub> using the uranium-reduction technique of Bigeleisen (1952), and analyzed for  $\delta$ D.

Initial  $d^{18}O_{H_2O}$  values were calculated using the following equation:

$$\delta^{18}O_{H_2O} = (\mu\text{molCO}_2/\mu\text{molH}_2\text{O}) (\delta^{18}O^f - \delta^{18}O^i) - \Delta + \delta^{18}O^f$$

where  $\delta^{18}O_{H_2O}$  is the initial oxygen isotopic water value,  $\delta^{18}O^f$  and  $\delta^{18}O^i$  are the final and initial CO<sub>2</sub> values in permil relative to SMOW.  $\Delta$  was calculated from the CO<sub>2</sub>/H<sub>2</sub>O fractionation factor (Friedman and O'Neil, 1977) at a known temperature.  $\mu\text{molCO}_2$  and  $\mu\text{molH}_2\text{O}$  are the amounts of CO<sub>2</sub> and water respectively. Quantities of H<sub>2</sub> produced from equilibrated waters were measured in the uranium reduction



A range of experiments using standard waters has yielded an average  $H_{me}$  value of 8.0 (See Table 2).

As can be seen from inspection of equation (1) and Table 3, smaller samples are more influenced by memory effect than are larger ones. This is because a constant number of hydrogen atoms ( $H_{me}$ ) exchanges with each sample water regardless of sample size. Residual hydrogen in the line may be stored as adsorbed  $H_2O$  or as uranium hydrides or both. The  $H_{me}$  value may decrease while the line is idle and  $H_2O$  desorbs from internal surfaces. However, this occurs slowly and  $H_{me}$  will return to its normal value as soon as any water is introduced into the line.

In order to correct  $\delta D$  values using equation (1),  $\delta D_p$  must be known. Therefore, a blank should be run at the start of each sample processing day in order to establish a  $\delta D_p$  value for use in correcting the measured  $\delta D$  of the first unknown sample. The in-house distilled water standard is a good water to use for this purpose. The uncorrected  $\delta D$  of this blank should be within about 4% of the actual value. For waters with similar  $\delta D$  values, the magnitude of memory effect is small to negligible. For consecutively run samples with a large range in  $\delta D$ , memory effect can be quite substantial. As a result, accuracy and precision are best ( $\pm 2\%$ ) for consecutively run samples with similar  $\delta D$ , and poor for widely ranging samples. In some cases, where consecutively run samples have a large difference in  $\delta D$ , or significantly differ isotopically from the in-house standard

water, it may be necessary to precondition the line with a "blank" of the sample water of interest.

### *Toepler pump*

Because hydrogen is non-condensable in liquid nitrogen, a Toepler pump is required to quantitatively move  $H_2$  from the furnace into a sample bottle. The toepler pump utilizes mercury which is cycled between the Hg reservoir bulb and the gas reservoir bulb and  $H_2$  inflow tube. The cycling is controlled by a rough pump and a control box containing two electronically controlled vacuum valves.

When the pump valve is open and the air valve is closed, the mercury is fully contained in the Hg reservoir bulb. In this position, the pressure in the head space is less than or equal to that of the  $H_2$  inflow tube and hydrogen will flow freely into the gas reservoir bulb. The control box will close the pump valve and open the air valve after a few seconds in this position. At this point, air enters the head space displacing mercury into the gas reservoir bulb and the  $H_2$  inflow tube. This isolates the gas in the gas reservoir bulb as the mercury rises above the branch in the pump. As the mercury continues to rise, it pushes hydrogen past the "one-way" valve and into the small volume above it. This volume may or may not include the sample bottle depending on the positions of the stopcocks above the "one-way" valve. As the mercury contacts the lead above this valve, it closes a circuit which causes the

control box valves to reverse and the mercury to fall as the head space is evacuated. Hydrogen is again allowed to flow freely from the H<sub>2</sub> inflow tube as the cycle repeats.

### *Procedure*

1. Start Hg diffusion pump. First, turn on cooling water and fill bulb with liquid nitrogen. Turn on variac and set at 45. Let pump work for at least 15 minutes before processing any waters.

2. Introduce water into line. To do this, seal about 5mg of water into a capillary tube and load it into the capillary breaker. Evacuate all parts of the vacuum line including capillary breaker, Toepler pump, and sample bottle. Shut the valve immediately above the capillary breaker and break the capillary tube. Using liquid nitrogen, transfer the released water into the double U-trap. After at least one minute, leaving the liquid nitrogen on the trap, open the valves downstream of the double U-trap, to the vacuum pumps, thereby removing any non-condensable gases.

3. Process water. Close the valve immediately upstream of the double U-trap, all valves to the vacuum pumps, and the valves on either side of the detour. Start the Toepler pump. Move the liquid nitrogen from the double U-trap to the single U-trap. Do not heat the double U-trap; allow it to warm slowly. When most of the sample has been converted to H<sub>2</sub>, open both valves on the detour and close

the valve immediately right of the single U-trap. Remove the liquid nitrogen and allow the trap to warm. When the single U-trap has warmed to room temperature, use a heat gun to remove the condensation inside the trap.

4. Measure yield. When "all"\* of the water has been processed and collected (probably about 15 minutes after removal of liquid nitrogen from single U-trap), manually operate the Toepler pump so that the bottom of the Hg meniscus is at the calibration mark at the bottom of the frosted glass. Measure the yield.

5. Bottle hydrogen. Allow the mercury to rise to the base of the lowest stopcock (T1) thereby minimizing the volume occupied by the H<sub>2</sub>. Close the sample bottle and stopcock T2 and pull the mercury back into the reservoir bulb. Remove the sample bottle and measure the H<sub>2</sub> on the mass spectrometer.

\* Due to the nature of the Toepler pump, 100% of the hydrogen cannot be collected. The small amount of water that passes through the uranium furnace without being converted to H<sub>2</sub> is collected in the single U-trap. This water is strongly fractionated from the bulk composition. Therefore, it is important to retrieve most of the H<sub>2</sub> produced from this water (the last H<sub>2</sub> to be produced). If the hydrogen produced from this water is not collected, the analyzed value will be too light.

### *Uranium furnace*

Depleted uranium turnings are used as a reaction medium in the reduction process. The release of  $H_2$  occurs above  $750^\circ C$ . Therefore, it is essential that all of the uranium is at or above this temperature. The furnace is hottest at the bottom and coolest at the top, with a temperature gradient of as much as  $100^\circ C$  over this distance. Because of this, the thermocouple should be placed at the top of the uranium which should not extend above the top of the heating element.

As more water is processed, the uranium becomes increasingly oxidized. Because this reaction utilizes only the surfaces of the metal, it is important that they are well cleaned prior to packing of the uranium furnace. Follow these steps to prepare a uranium furnace:

- (1) Crush uranium (about 30 g) in liquid nitrogen with a mortar and pestle.
- (2) Bathe uranium in warm 1N nitric acid for about 15 minutes (until surface oxidation is removed) and rinse in distilled water.
- (3) Soak uranium in acetone and rinse in distilled water.
- (4) Soak copper in acetone and rinse in distilled water.
- (5) Dry uranium and copper in low temperature oven.
- (6) Clean quartz tube in nitric acid and rinse in

distilled water.

(7) Pack furnace as shown in diagram, taking care not to touch copper, quartz wool, or uranium.

The lifetime of a uranium furnace should be about 90 working days. Watch for yellowish-brown residues creeping up the furnace tube toward the end of its life. Memory effect should become more pronounced toward the end of a furnace's life.

lab number	$\delta D_s$	$\delta^{18}O_{H_2O}$	mg H <sub>2</sub> O
HU/CO <sub>2</sub> 29-1	-1.9	0.6	10
HU/CO <sub>2</sub> 29-2	-0.9	0.3	10
HU/CO <sub>2</sub> 29-3	-3.7	-1.5	5
HU/CO <sub>2</sub> 29-4	-1.2	1.0	5
HU/CO <sub>2</sub> 29-5	-4.8	1.5	3
HU/CO <sub>2</sub> 29-6	-5.7	0.9	3
HU/CO <sub>2</sub> 32-1	-4.2	-0.3	5
HU/CO <sub>2</sub> 32-2	-2.2	0.5	5
HU/CO <sub>2</sub> 32-3	-5.5	-0.7	5
HU/CO <sub>2</sub> 32-4	-8.6	-0.8	5
average	-3.87	0.15	
standard deviation	2.28	0.89	
maximum error (2 $\sigma$ )	4.6	1.8	

Table 1. Isotopic values of SMOW standard waters in which single aliquots were microequilibrated and subsequently reduced by uranium. These values are used to assign errors to all  $\delta D$  and  $\delta^{18}O$  data. In addition, the low  $\delta D_s$  values measured in microequilibrated SMOW, justify the addition of 4 permil to  $\delta D_s$  values.

Sample number	Standard	$\delta D_m$	$\delta D_p$	$H_s$ ( $\mu$ moles)	$H_{me}$ ( $\mu$ moles)
HU-5-6	SMOW	-2.56	-81.15	194	6.3
HU-6-5	SMOW	-4.31	-83.19	128	7.0
HU-6-7	GISP	-186.68	-80.02	272	8.0
HU-7-13	SMOW	-3.07	-23.51	72	10.8

Table 2. Values from standard waters used to calculate average  $H_{me}$ .

Sample number	Standard	mg water	$\delta D_m$	$\delta D_p$	$\delta D_s$
HU-5-1	SMOW	4.7	-1.8		
HU-5-2	SMOW	3.0	-1.1	-1.8	-1.1
HU-5-3	SMOW	6.3	0.9	-1.1	0.9
HU-5-6	SMOW	3.5	-2.6	-81.2	0.6
HU-5-7	SMOW	3.8	-1.5		
HU-6-5	SMOW	2.3	-4.3	-83.2	0.6
HU-6-7	GISP	4.9	-186.7	-80.0	-189.8
HU-6-8	SMOW	3.5	-1.8		
HU-7-1	SMOW	1.4	-5.6		
HU-7-13	SMOW	1.3	-3.1	-23.5	-0.8

Table 3. Data for standards run before 6 September 1993.

Samples without  $\delta D_p$  and  $\delta D_s$  values were run at the start of the processing day.  $\delta D_s$  values are corrected values using  $H_{me} = 8.0$ . No corrections based on HD-1, HD-2, and HD-3 are applied. These waters were not subjected to the microequilibration procedure prior to uranium reduction.

This document is accepted on behalf of the faculty  
of the Institute by the following committee:

Andrew Campbell

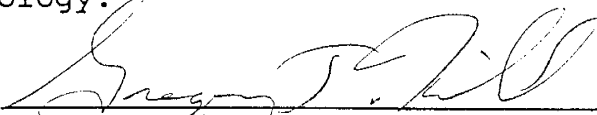
Adviser

Philip Kyle by David B. Johnson

William J. Chavez, Jr. 5 October, 1994

Date

I release this document to New Mexico Institute of Mining and  
Technology.

  
Students Signature

4 OCT 94  
Date